Supporting Information: Novel Zero-dimensional Lead-free Bismuth Based Perovskites: From Synthesis to Structural and Optoelectronic Characterization

Mailde S. Ozório,*,† Willian X. C. Oliveira,*,‡ Julian F. R. V. Silveira,*,† Ana Flávia Nogueira,*,¶ and Juarez L. F. Da Silva*,†

†*São Carlos Institute of Chemistry, University of São Paulo, PO Box* 780, 13560-970, *São Carlos, SP, Brazil*

‡*Departamento de Química, Instituto de Ciências Exatas, Universidade Federal de Minas Gerais, PO Box* 6154, 13083-970, *Belo Horizonte, MG, Brazil*

¶*Institute of Chemistry, University of Campinas, PO Box* 6154, 13083-970 *Campinas, SP, Brazil*

E-mail: mailde.s.ozorio@usp.br; wxcoliveira@ufmg.br; juliansilveira@usp.br; anafla@unicamp.br; juarez_dasilva@iqsc.usp.br

1 Introduction

The present electronic supporting information is separated into two sections, namely, Experimental and theoretical sections, which provide additional details on the experiments and

calculations, as well as additional data to support our conclusions. Furthermore, additional details can be obtained directly with the authors.

1.1 Ultraviolet-visible spectra

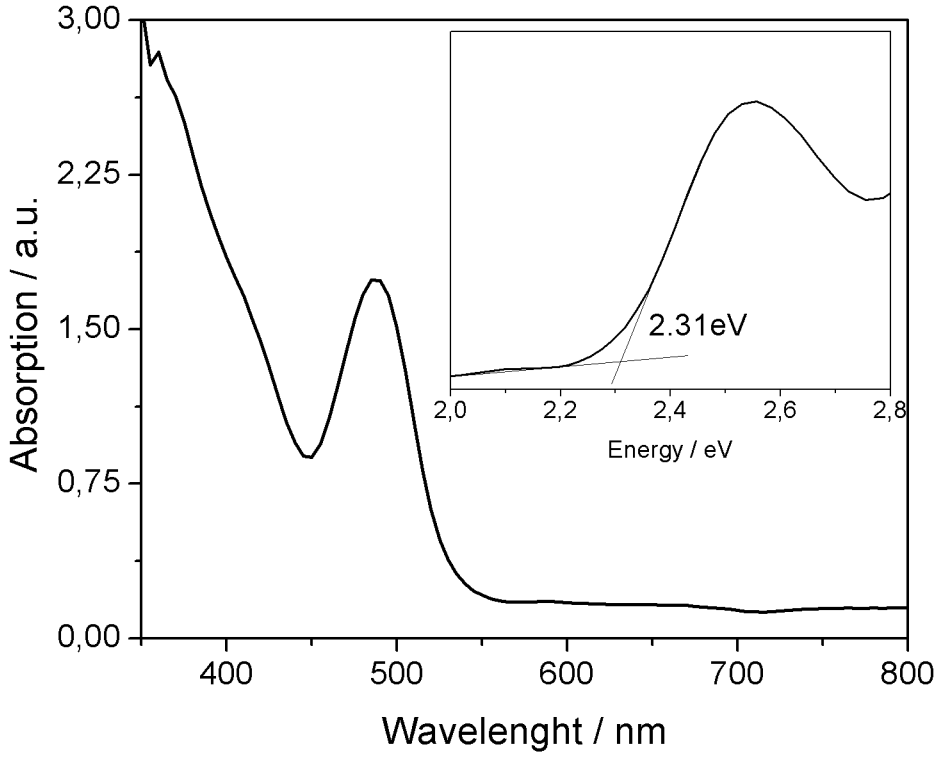

Figure S1: UV-vis absorption spectra of the 1 perovskite in thin film. Inset is direct optical band gap obtained by the Tauc plot for an direct allowed transition.

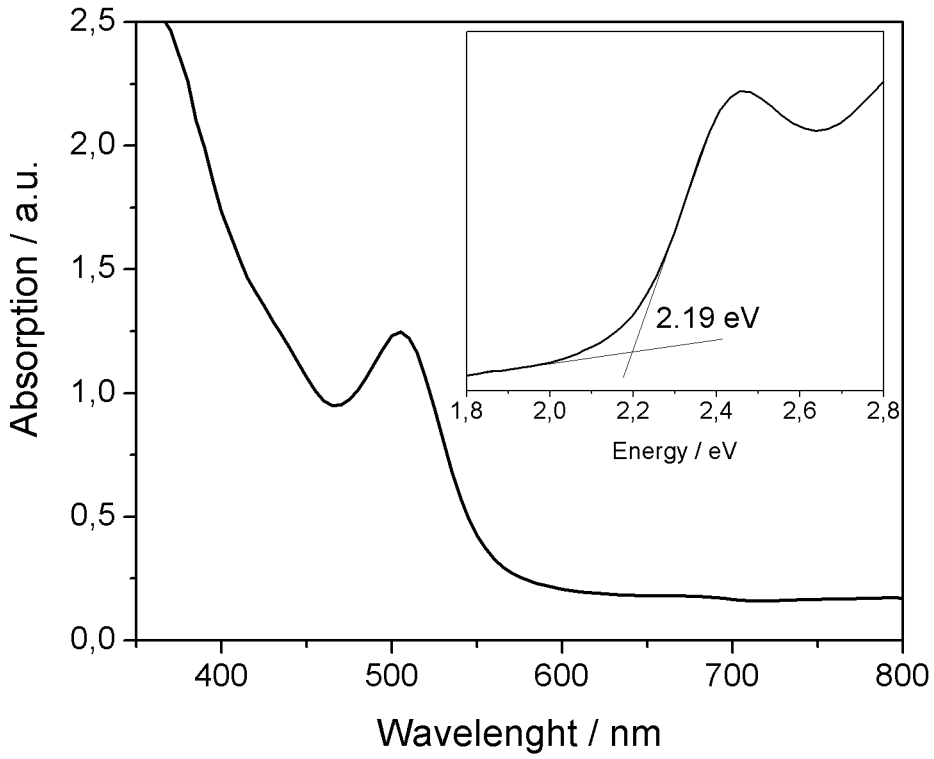

Figure S2: UV-vis absorption spectra of 2 perovskite in thin film. Inset is direct optical band gap obtained by the Tauc plot for an direct allowed transition.

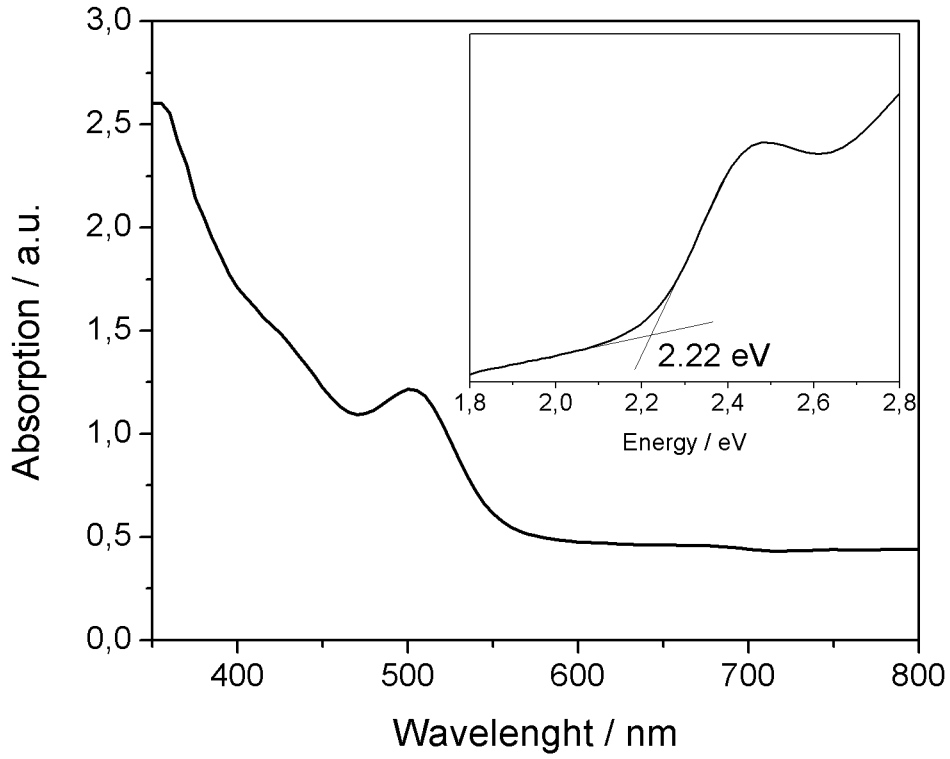

Figure S3: UV-vis absorption spectra of 3 perovskite in thin film. Inset is direct optical band gap obtained by the Tauc plot for an direct allowed transition.

1.2 Photoluminescence spectra

All three zero-dimensional perovskites did not presented photoluminescence detectable in the range of 400 and 650 nm. Artifacts can be found around 450 and 530 nm, associated to inelastic scattering caused by thin film surface.

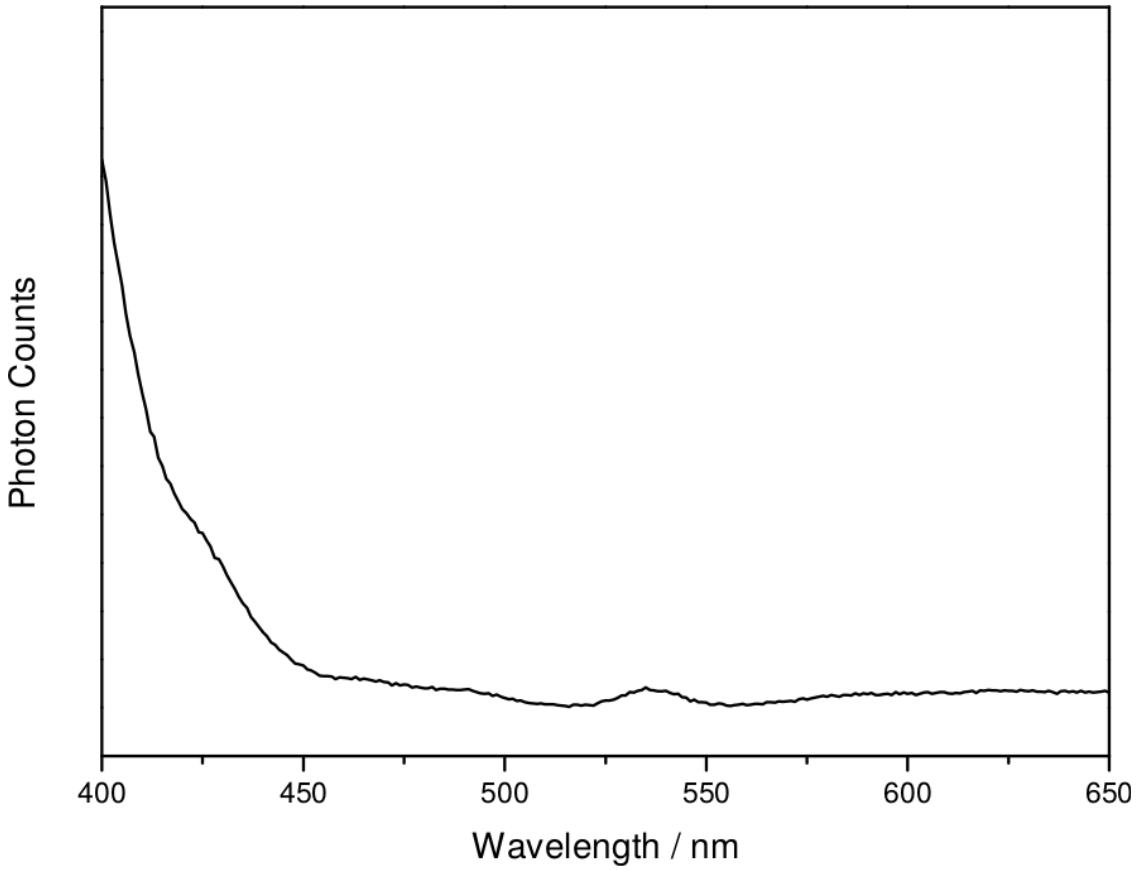

Figure S4: Photoluminescence spectra of 1 perovskite in thin film.

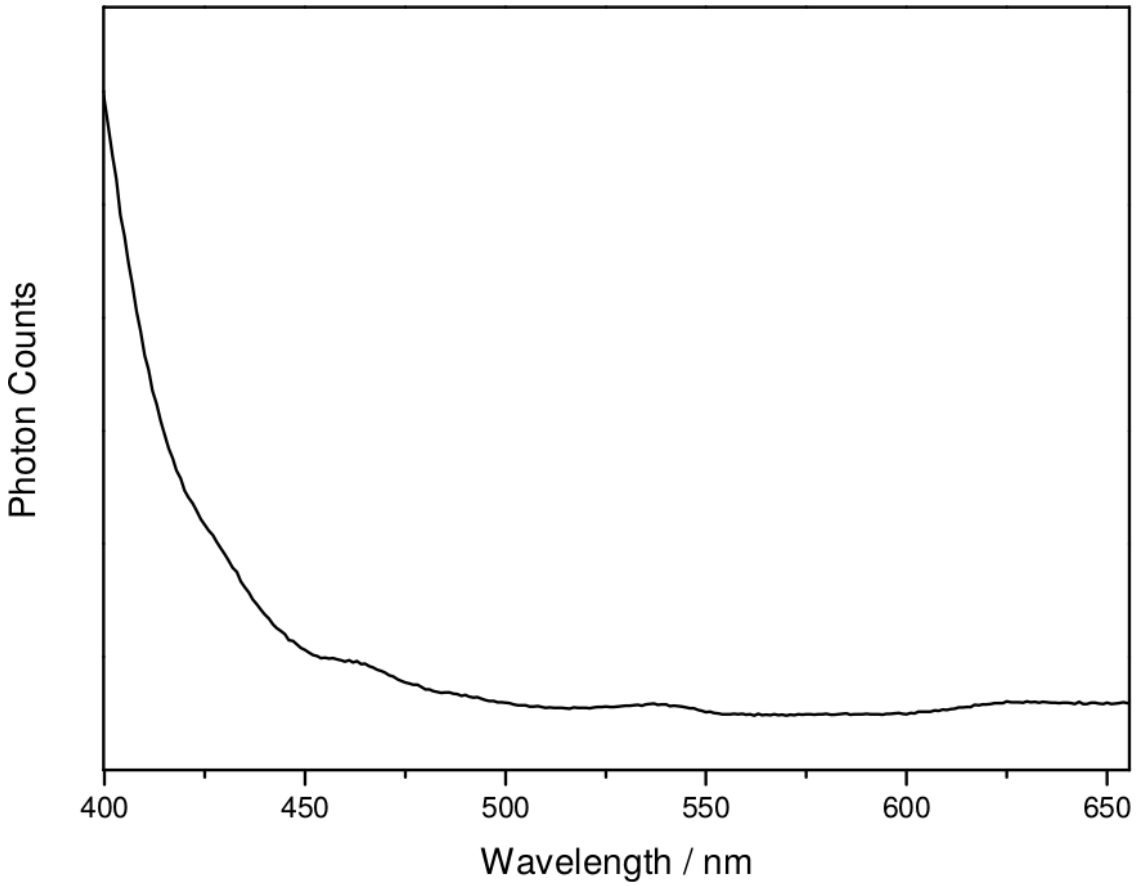

Figure S5: Photoluminescence spectra of 2 perovskite in thin film.

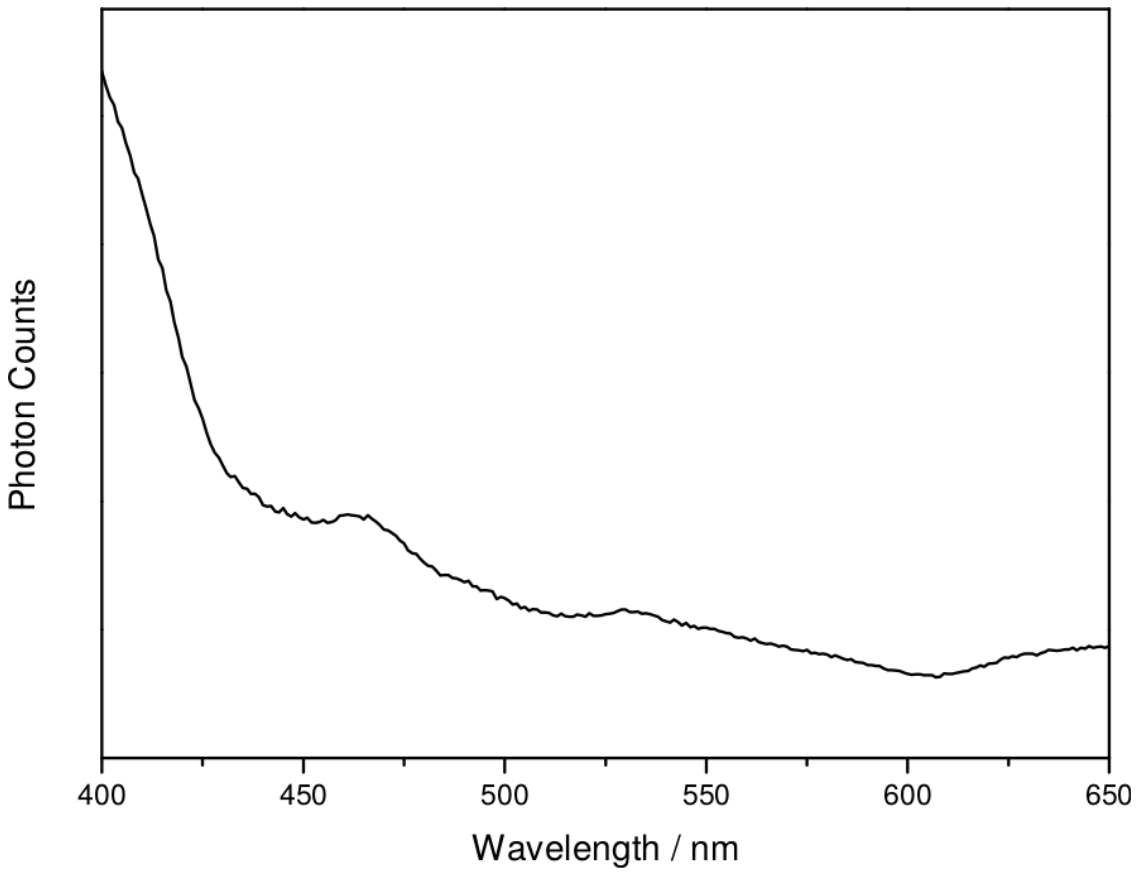

Figure S6: Photoluminescence spectra of 3 perovskite in thin film.

Table S1: Summary of the crystal data and refinement parameters for the 1, 2 and 3 zero-dimensional perovskites.

Compounds	**1**	**2**	**3**
Chemical Formula	$C_{20}H_{20}N_4Bi_2I_{10}$	$C_{42}H_{39}N_6Bi_2I_9$	$C_{30}H_{25}N_6BiI_6 \cdot 2\,H_2O$
F_w ($g\,mol^{-1}$)	2003.36	2187.85	1475.97
λ (Å)	0.710 73	0.71073	0.71073
Crystal size (mm^3)	0.28×0.15×0.07	0.17×0.10×0.08	0.39×0.17×0.07
Crystal system	Triclinic	Orthorhombic	Triclinic
Space Group	$P\bar{1}$	$Pna2_1$	$P\bar{1}$
a / Å	8.8336(8)	23.5530(16)	10.666(2)
b / Å	10.7018(10)	10.4348(7)	10.822(2)
c / Å	11.7936(10)	21.9237(15)	10.947(2)
α / °	114.450(2)	90	81.045(4)
β / °	99.704(2)	90	61.715(2)
γ / °	100.092(2)	90	61.460(4)
Volume / $Å^3$	962.40(15)	5388.2(6)	973.4(3)
T/ K	150(2)	150(2)	290(2)
Z	1	4	1
$F(000)$	864	3904	668
hkl range	-11 ≤ h ≤ 10	-29 ≤ h ≤ 29	-13 ≤ h ≤ 13
	-13 ≤ k ≤ 13	-13 ≤ k ≤ 13	-13 ≤ k ≤ 13
	-14 ≤ l ≤ 14	-27 ≤ l ≤ 27	-13 ≤ l ≤ 13
ρ_{calc} / $g\,cm^{-3}$	3.457	2.697	2.518
μ / mm^{-1}	17.168	11.714	9.320
Collected reflections	10537	77406	26083
Independent reflections	3935	11011	3994
Reflections with $I \geq 2\sigma(I)$	3840	10653	3913
R_{int}	0.013	0.012	0.016
R[1]; wR[2] [$I \geq 2\sigma(I)$]	0.027;0.072	0.027;0.079	0.036;0.090
R^a; wR^b (all data)	0.028; 0.072	0.028; 0.080	0.036; 0.091
Goodness-of-fit on F^2 (S[3])	1.122	0.984	1.129
Larg. diff. peak and hole/e $Å^{-3}$	1.95,-2.69	1.18,-0.74	3.10,-1.20
Mean residual electronic density/e $Å^{-3}$	0.32	0.11	0.20

Table S2: Symmetry code information for 1 zero-dimensional perovskite.

Bi–I (Å)		I–Bi–I (°)	
Bi1–I1	2.9640(4)	I1–Bi1–I2	91.184(11)
Bi1–I2	2.9889(4)	I1–Bi1–I3	174.821(10)
Bi1–I3	3.2062(4)	I1–Bi1–I3^{i}	90.346(11)
Bi1–I3^{i}	3.2562(4)	I1–Bi1–I4	89.969(10)
Bi1–I4	3.1503(4)	I1–Bi1–I5	96.357(12)
Bi1–I5	2.9508(4)	I2–Bi1–I3	90.245(10)
		I2–Bi1–I3^{i}	88.732(12)
Intracomplex Bi···Bi (Å)		I2–Bi1–I4	176.253(10)
Bi1···Bi1^{i}	4.7758(5)	I2–Bi1–I5	91.038(13)
		I3–Bi1–I3^{i}	84.709(11)
Intermolecular I···I (Å)		I3–Bi1–I4	88.298(10)
I2···I2^{iii}	4.2045(7)	I3–Bi1–I5	88.592(12)
I4···I4^{v}	4.9860(6)	I4–Bi1–I3^{i}	87.696(12)
I5···I5^{iv}	4.5573(5)	I4–Bi1–I5	92.377(12)
		I5–Bi1–I3^{i}	173.296(11)
Hydrogen bonds (Å)			
N1–H1···I3	2.921	Bi–I–Bi (°)	
N2–H2···I4^{ii}	3.086	Bi1–I3–Bi1^{i}	95.291(11)
Symmetry codes: i = 1-x, 2-y, 1-z; ii = 1+x, -1+y, -1+z; iii = 1-x, 1-y, 1-z; iv = 1-x, 2-y, 2-z; v = 1-x, 3-y, 2-z.			

Table S3: Symmetry code information for 2 zero-dimensional perovskite.

Bi–I (Å)		I–Bi–I (°)	
Bi1–I1	2.9009 (9)	I1–Bi1–I2	88.77 (3)
Bi1–I2	3.0045 (9)	I1–Bi1–I3	96.65 (3)
Bi1–I3	2.9704 (9)	I1–Bi1–I4	90.89 (2)
Bi1–I4	3.2999 (9)	I1–Bi1–I5	90.42 (3)
Bi1–I5	3.1472 (8)	I1–Bi1–I6	170.29 (3)
Bi1–I6	3.2987 (8)	I2–Bi1–I3	91.42 (3)
Bi2–I4	3.2192 (8)	I2–Bi1–I4	99.44 (3)
Bi2–I5	3.2896 (8)	I2–Bi1–I5	177.61 (3)
Bi2–I6	3.3589 (9)	I2–Bi1–I6	93.16 (2)
Bi2–I7	2.9263 (9)	I3–Bi1–I4	166.92 (3)
Bi2–I8	2.8970 (9)	I3–Bi1–I5	86.43 (3)
Bi2–I9	3.0125 (9)	I3–Bi1–I6	92.81 (2)
Intracomplex Bi···Bi (Å)		I4–Bi1–I5	82.83 (2)
Bi1···Bi2	4.2175(7)	I4–Bi1–I6	79.41 (2)
		I5–Bi1–I6	88.01 (2)
Intermolecular I···I (Å)		I4–Bi2–I5	81.90 (2)
I1···I8^{i}	3.367	I4–Bi2–I6	79.68 (2)
I7···I2^{iii}	4.031	I4–Bi2–I7	94.95 (3)
		I4–Bi2–I8	91.30 (3)
Hydrogen bonds (Å)		I5–Bi2–I9	171.09 (3)
N2–H2···I6	3.235	I5–Bi2–I6	84.71 (2)
N3–H3···I3^{i}	2.943	I5–Bi2–I7	88.97 (3)
N3–H5···I9^{ii}	3.278	I5–Bi2–I8	172.70 (3)
		I4–Bi1–I5	93.30 (2)
Bi–I–Bi (°)		I6–Bi2–I7	172.21 (3)
Bi1–I4–Bi2	80.615 (19)	I6–Bi2–I8	91.50 (3)
Bi1–I5–Bi2	81.841 (19)	I6–Bi2–I9	92.44 (3)
Bi1–I6–Bi2	78.610 (17)	I7–Bi2–I8	94.27 (3)
		I7–Bi2–I9	92.46 (3)
		I8–Bi2–I9	93.08 (3)
Symmetry codes: i = -1/2+x, 1/2-y, z; ii = x, 1+y, z; iii = 3/2-x, -1/2+y, 1/2+z;			

Table S4: Symmetry code information for 3 zero-dimensional perovskite.

Bi–I (Å)		I–Bi–I (°)	
Bi1–I1	3.0899 (7)	I1–Bi1–I2	90.975 (17)
Bi1–I2	3.0738 (8)	I1–Bi1–I3	88.037 (17)
Bi1–I3	3.0800 (7)	I1–Bi1–I1^{i}	180
		I1–Bi1–I2^{i}	89.025 (17)
Hydrogen bonds (Å)		I1–Bi1–I3^{i}	91.962 (17)
N1–H1···O1	1.955	I2–Bi1–I3	87.718 (15)
N2–H2···O1	2.551	I2–Bi1–I2^{i}	180
N3–H3···O1	1.937	I2–Bi1–I3^{i}	92.282 (15)
O1–H1C···I1	3.029	I3–Bi1–I3^{i}	180
O1–H1C···I2	3.105		
O1–H1B···N1	1.794		
O1–H1A···N3	1.839		
Symmetry code: i = -x+1, -y+2, -z.			

Table S5: Average bond length of C−C (d_{C-C}), C−H (d_{C-H}), C−N (d_{C-N}), and N−H (d_{N-H}) present on the organic cation of 1, 2, and 3 experimental structures as well as the strongest hydrogen-bond $d_{H\cdots I}$ length.

	d_{C-C} (Å)	d_{C-H} (Å)	d_{C-N} (Å)	d_{N-H} (Å)	$d_{H\cdots I}$ (Å)
1	1.40	0.95	1.34	0.88	2.90
2	1.41	0.96	1.35	0.88	2.94
3	1.40	0.93	1.34	0.86	3.04

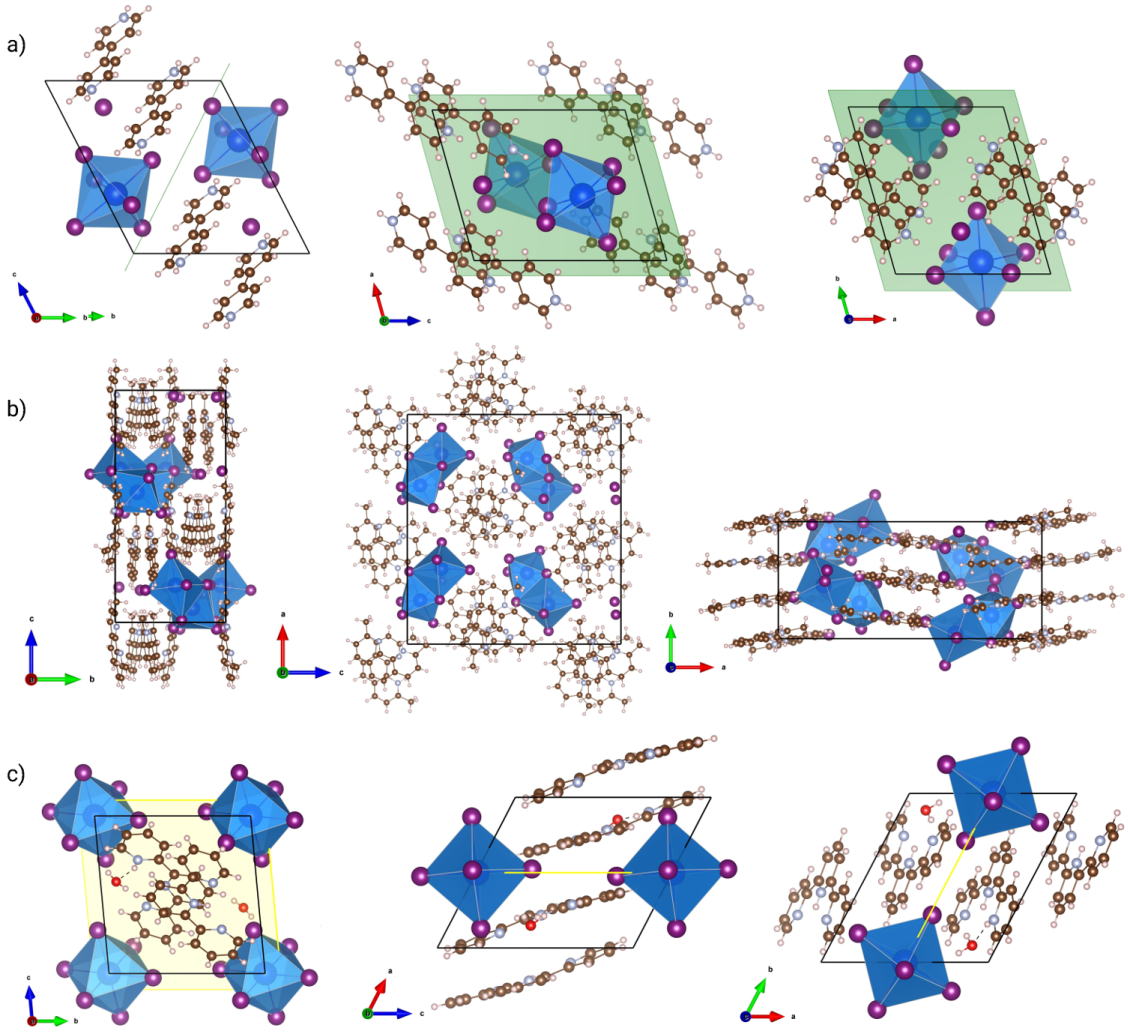

Figure S7: Different projections of experimental a) 1, b) 2, and c) 3 zero-dimensional perovskites.

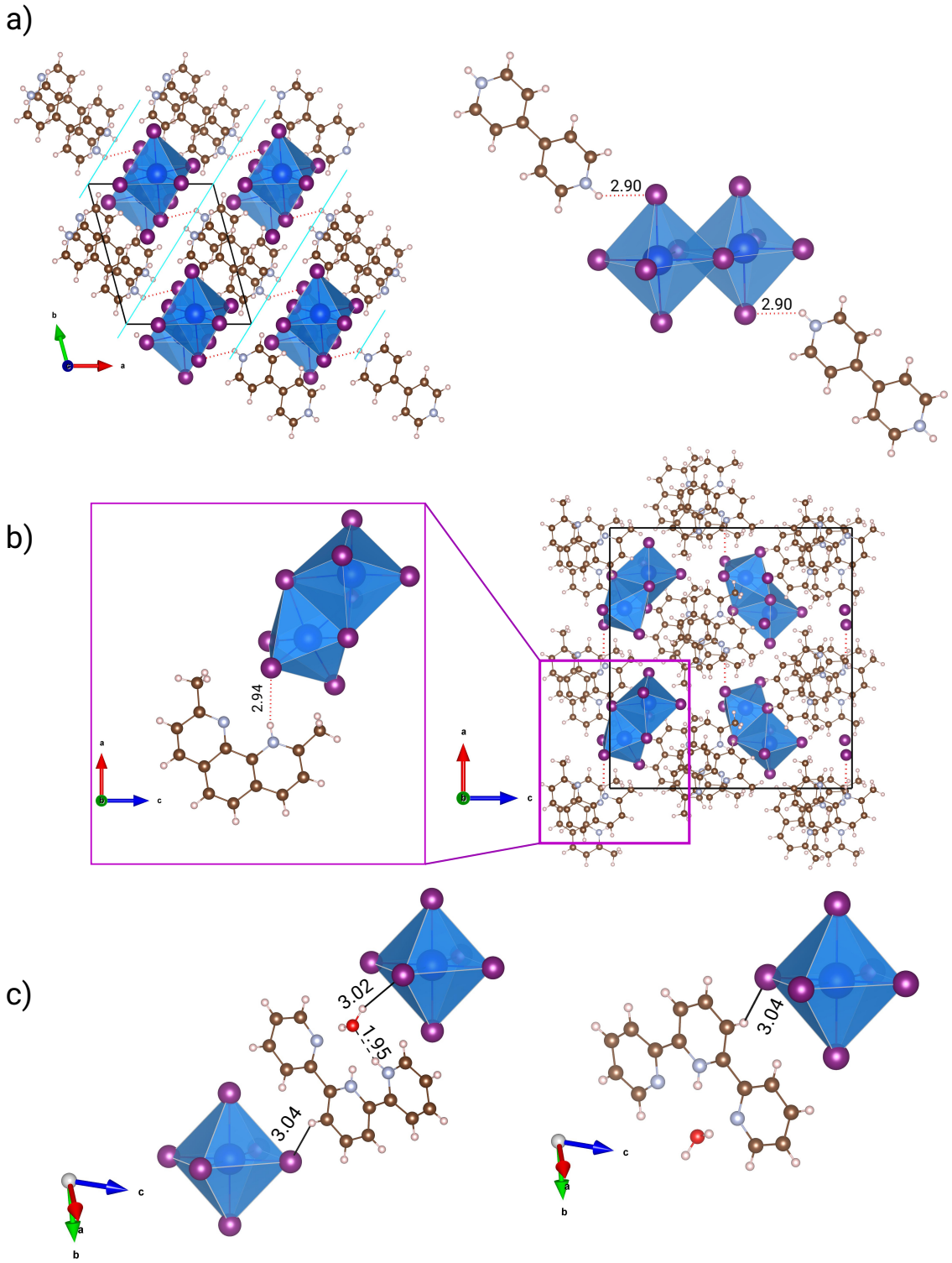

Figure S8: The lowest distance between iodine-hydrogen (hydrogen bonds) in the experimental a) 1, b) 2, and c) 3 perovskites.

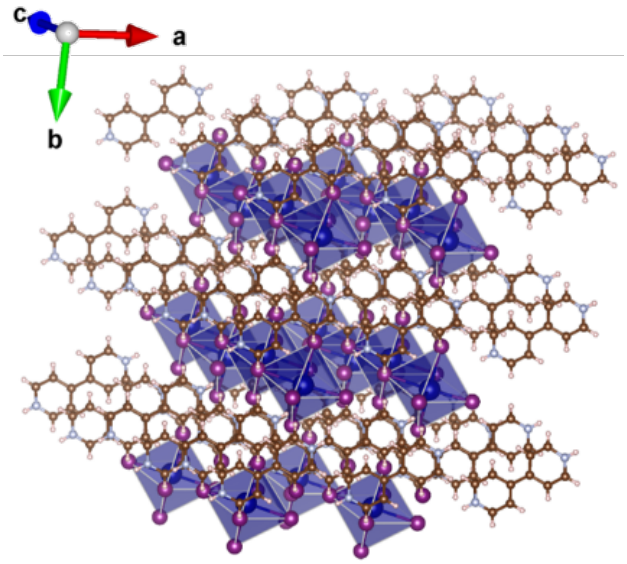

Figure S9: Crystal packing of 1 featuring the pseudo-2D perovskite like structure.

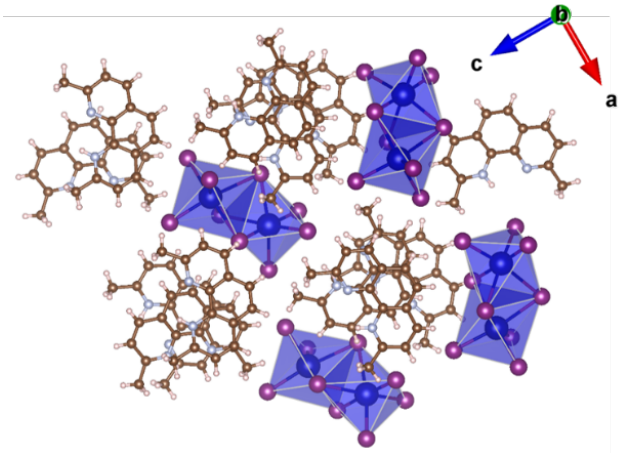

Figure S10: Crystal packing of 2 along crystallographic *b* axis, showcasing the π-stacking of Hdmphen$^+$ in a twisted arrangement.

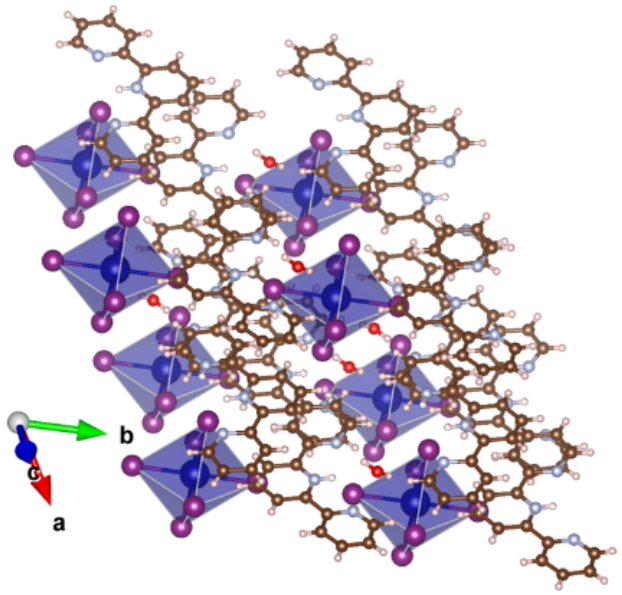

Figure S11: Crystal packing of 3 with a pseudo-1D perovskite like structure.

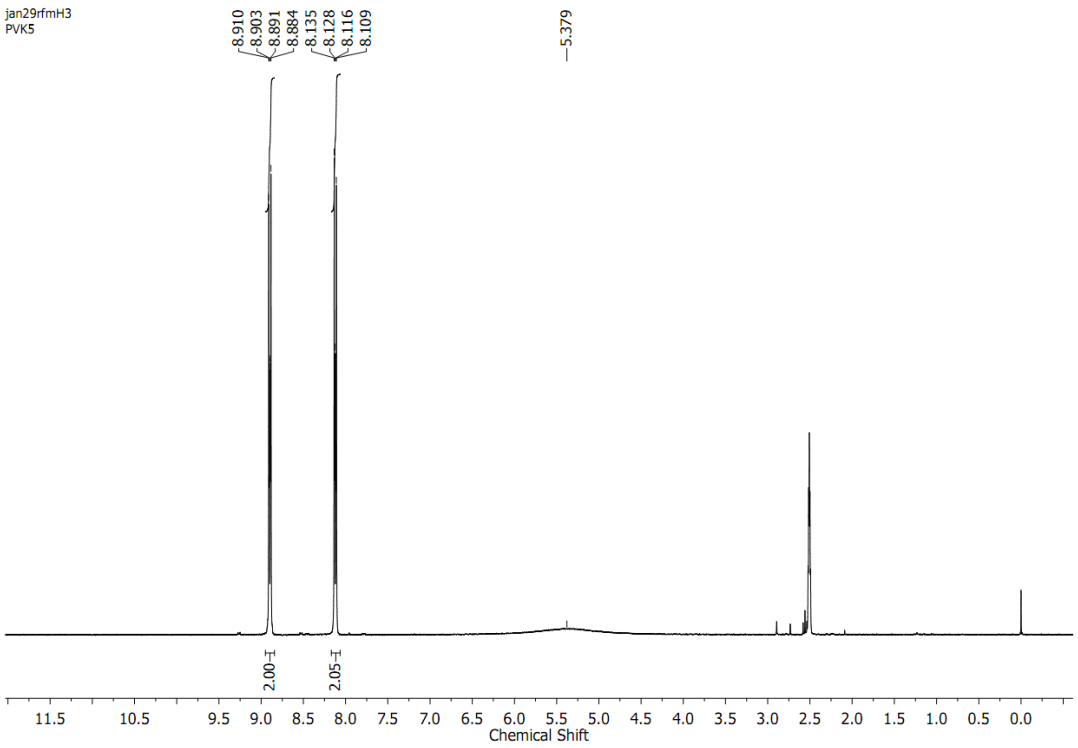

Figure S12: 1H NMR spectrum of 1.

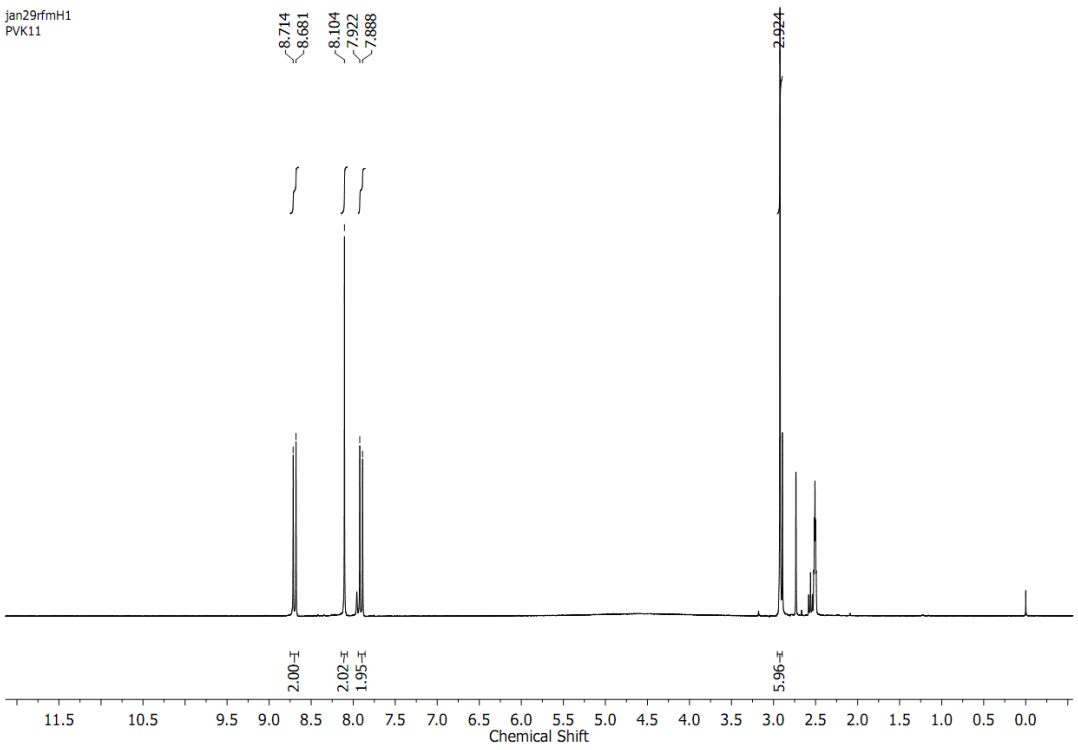

Figure S13: 1H NMR spectrum of 2.

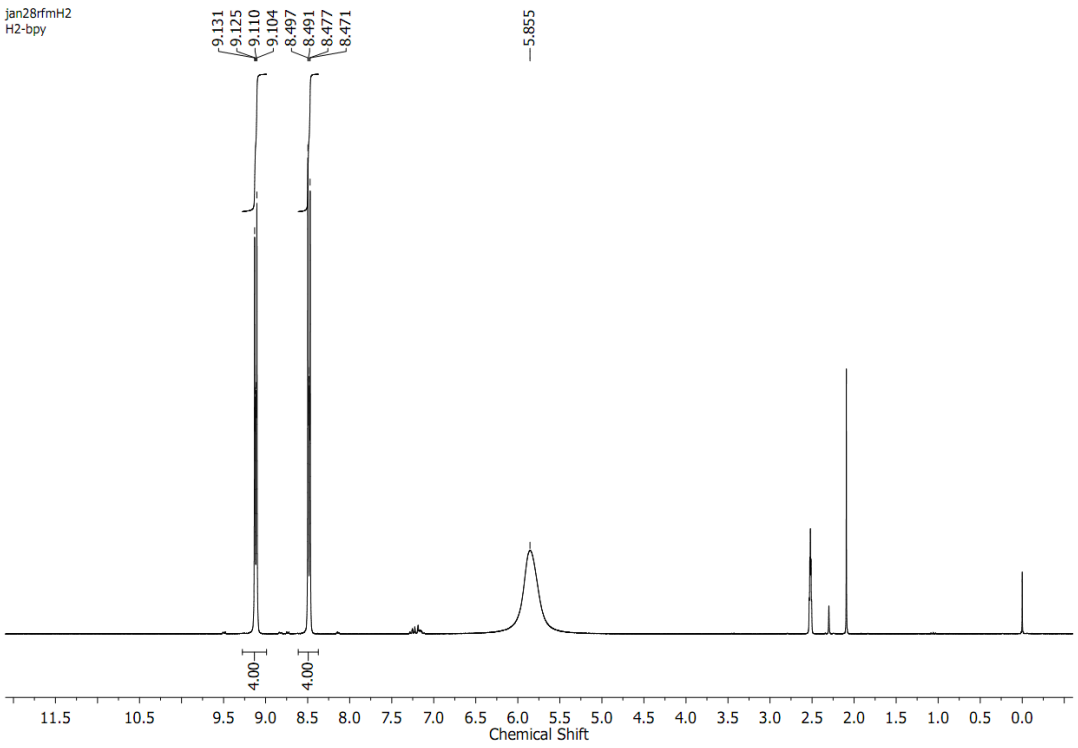

Figure S14: 1H NMR spectrum of 3.

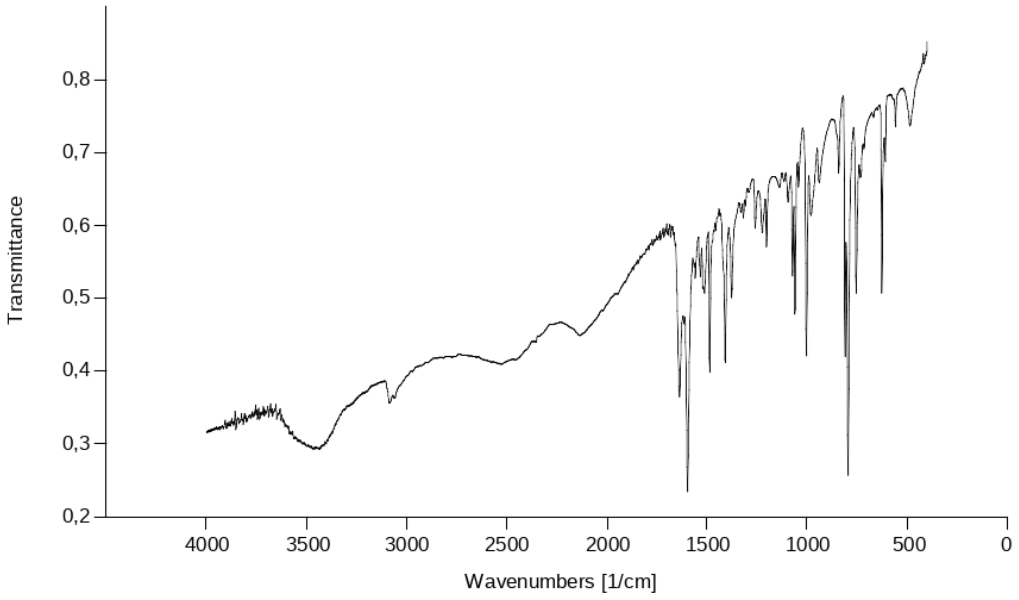

Figure S15: FTIR spectrum of 1.

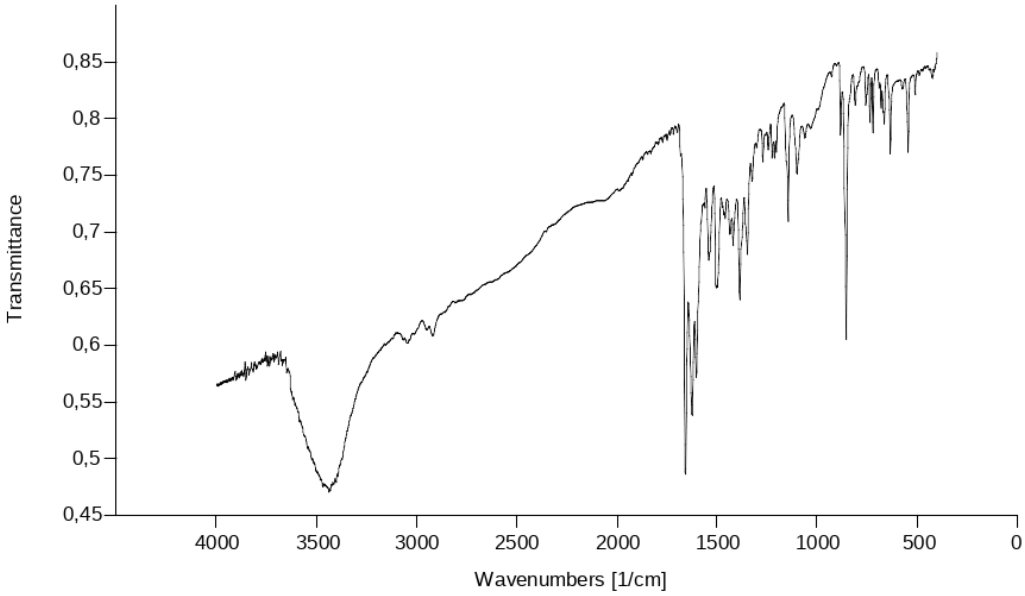

Figure S16: FTIR spectrum of 2.

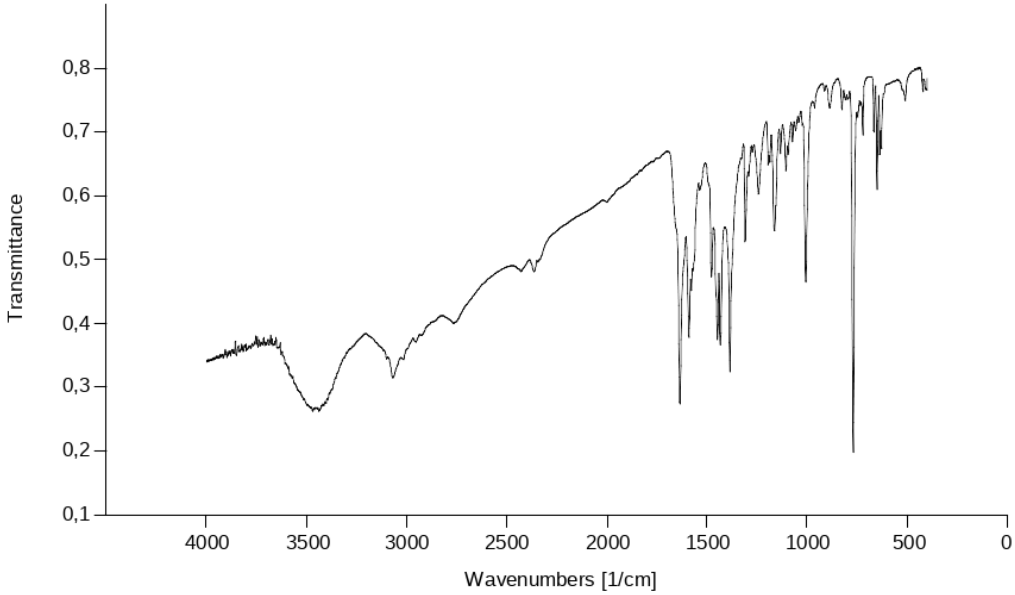

Figure S17: FTIR spectrum of 3.

1.3 Termogravimetric Analysis

1.3.1 Compound 1

Compound **1** is thermally stable from room temperature to 250 °C. In synthetic air, between 250 °C and 520 °C, three overlapped weight loss events occurred. It is associates to organic part decomposition and evaporation of most of bismuth(III) iodide (which occurs at 542 °C[S1]). The residual mass of this analysis is 4.1 %, which is probably a mixture between Bi_2O_3 and BiIO, products of oxidation of residual BiI_3.

1.3.2 Compound 2

2, in synthetic dry air, is thermally stable until 100 °C. Between 100 °C and 230 °C two weight losses are observed, with 13.0 % of mass loss, associated with two HI molecules (calculated for 2HI = 11.8 %). 230 °C forward several exothermic events occurred, associated with organic moieties decomposition and partially sublimation of bismuth atoms, reaching a plateau at630 °C with residual mass of 12.2 %.

1.3.3 Compound 3

Compound **3** under oxidizing atmosphere is thermally stable from room temperature until 130 °C. Between 130 °C and 220 °C two endothermic events with combined weight loss of 8.8 % can be associated to evaporation of two water molecules and one HI molecule (calculated = 9.2 %). Two other events take place between 630 and 360 °C with 59.2 % of weight loss. This loss is associated with organic moiety decomposition (calculated for residual BiI_3 = 37.2 %, found = 32.1 %). Between 360 °C and 420 °C the remaining material is thermally stable and then two other events occur, reaching a final residue at 645 °C with residual mass of 22.2 %. The final residue can be BiIO, which would correspond to 23.7 % of compound **3** mass.

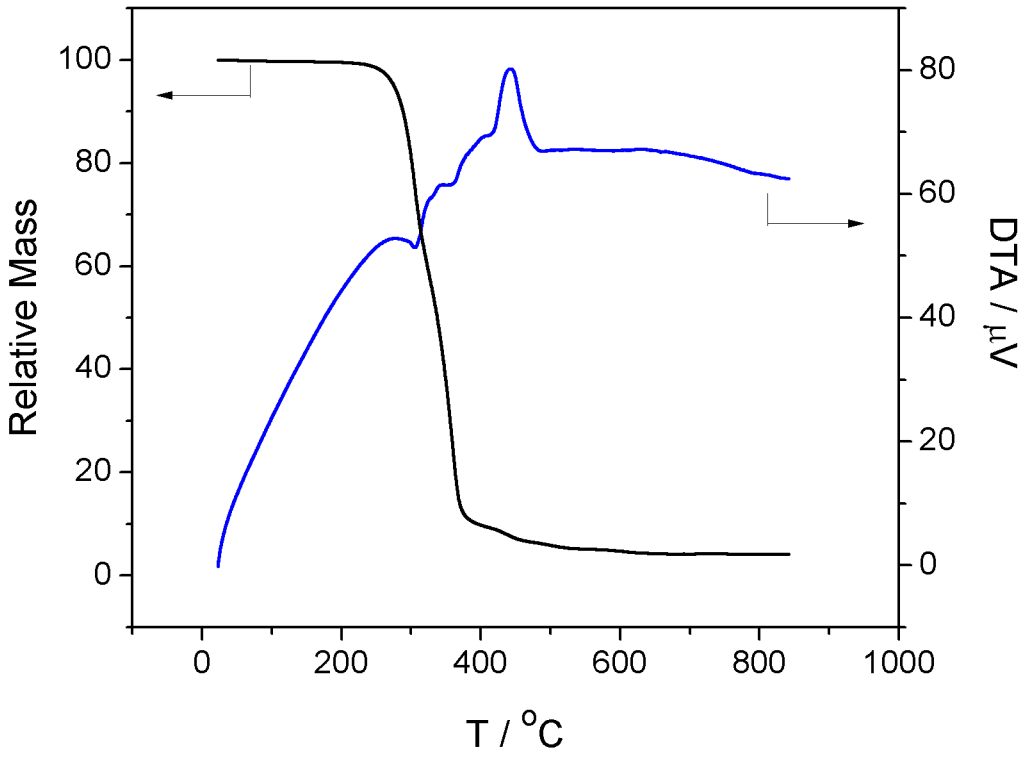

Figure S18: Relative mass perovskite of 1.

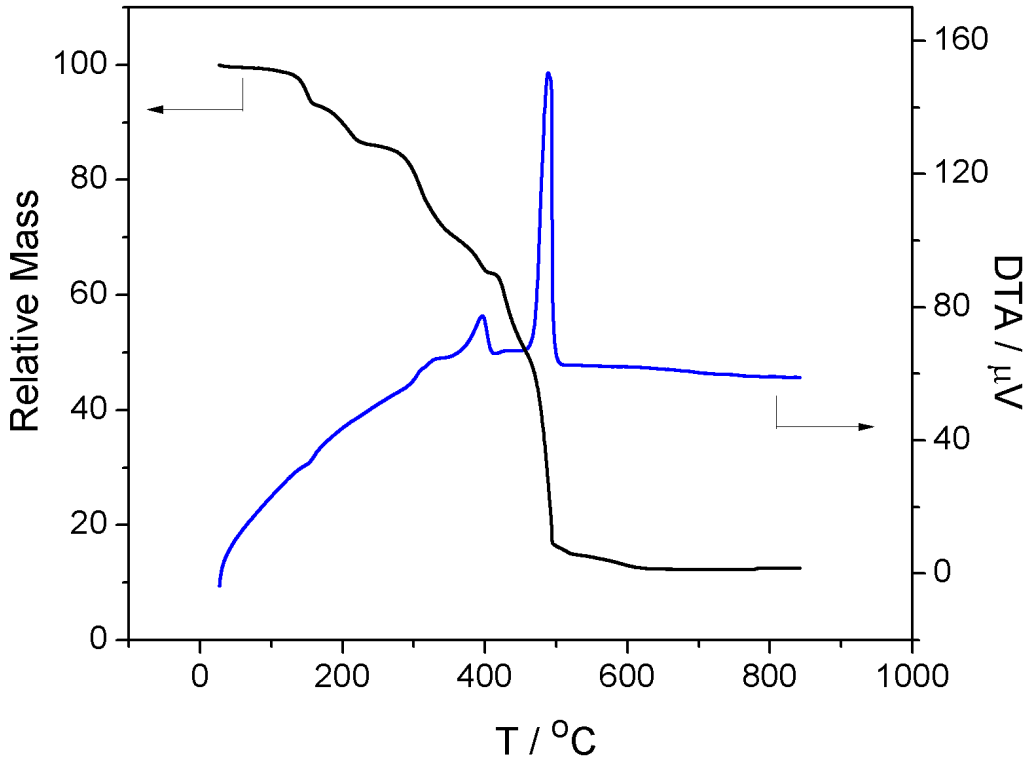

Figure S19: Relative mass perovskite of2.

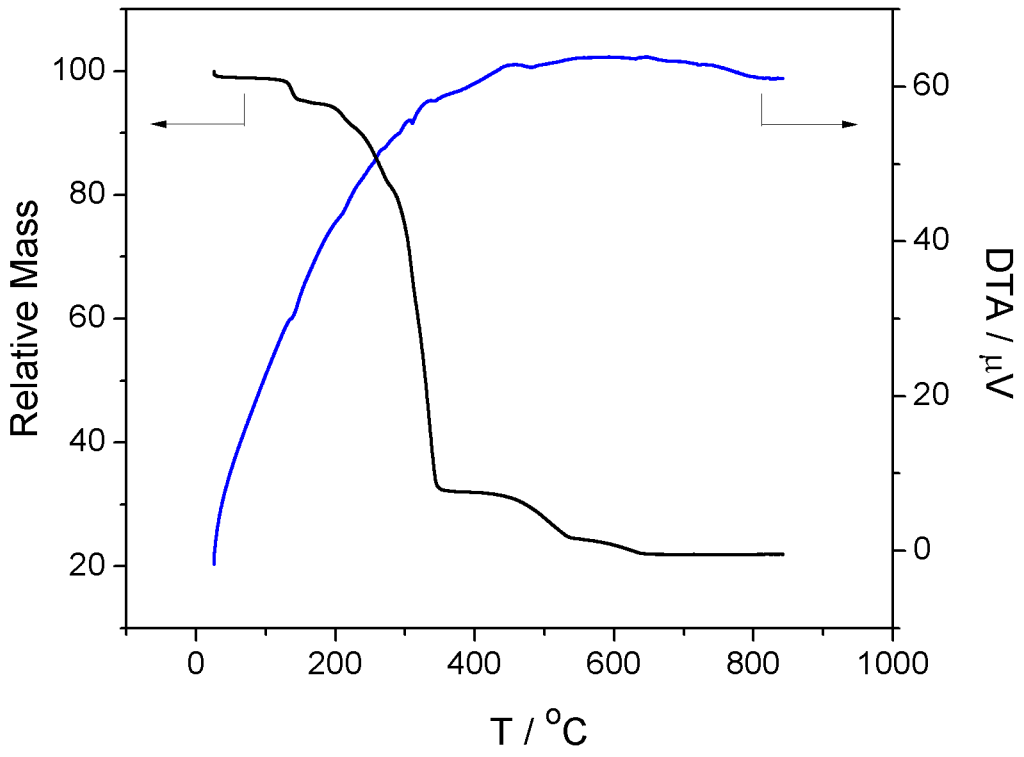

Figure S20: Relative mass perovskite of 3.

2 Theoretical Data and Analyses

2.1 Structural Parameters Definition

Given the geometric complexity of the hybrid perovskites under study, in order to get a better understanding of their structural properties, among other properties, we analyzed the main bonding lengths of the organic molecules, as well as the internal structural properties of the octahedrons, in which we considered the average and standard deviation values of I–Bi–I angles and Bi–I bond lengths. Beyond of the lattice parameters, a_0, b_0, c_0, we employed few additional parameters to characterize the local structures of the octahedra and organic molecules, namely, the effective coordination number of Bi (ECN^{Bi}) based on the effective coordination concept.[S2] Below, the most important parameters are define.

2.1.1 Effective Coordination Concept

The effective coordination number (ECN) concept[S2] was applied to account the effective number of iodide ions surrounding the Bi-cations in relatively distorted octahedra of the zero dimensional perovskites, labeled as **1**, **2** and **3**. Hence, in order to acquire the ECN^{Bi}, the following equation was applied:

$$ECN^{Bi} = \sum_j \exp\left[1 - \left(\frac{d_{ij}}{d^i_{av}}\right)^6\right], \qquad d^i_{av} = \frac{\sum_j d_{ij} \exp\left[1 - \left(\frac{d_{ij}}{d_{\min}}\right)^6\right]}{\sum_j \exp\left[1 - \left(\frac{d_{ij}}{d_{\min}}\right)^6\right]}, \tag{1}$$

where d_{ij} represent each Bi–I bond length of BiI_6 octahedral, the d^i_{av} represent a weighted average bond length, and $d_{\min}$ the smallest Bi–I bond-length among all six present in the BiI_6 moeity.

2.1.2 Bond Angle Variance

The bond angle variance (BAV) was applied to characterize the changes of IBiI angles in each BiI_6 octahedral. As proposed by Robinson *et al.*,[S3] the BAV values were obtained by the following equation:

$$BAV = \frac{1}{n-1}\sum_{i=1}^{n}(\phi_i - \phi_0)^2, \qquad BAV = \sum_{i=1}^{12}\frac{(\phi_i - 90^\circ)^2}{11} \tag{2}$$

where n is the number of faces multiplied by 3/2, thus in the octahedron $n = 12$, which is the total number of ϕ_i angles involving the bismuth and two adjacent iodide atoms, I–Bi–I, which in a perfect octahedron are all equal to $\phi_0 = 90^\circ$.

2.1.3 Distortion Index

The Distortion Index (DI)[S4] was obtained by applying the following equation:

$$\mathrm{DI} = \frac{1}{6}\sum_{i=1}^{6}\frac{|d_{ij} - d_{av}^{i}|}{d_{av}^{i}}\ , \tag{3}$$

where d_{ij} represent the distance from Bi-cation to the ith iodide ion of BiI_6 octahedral, while d_{av} represent the average Bi−I bond length.

2.1.4 Tests for the undermined hydrogen atoms position in the 3 perovskites

Table S6: Experimental and theoretical values of lattice parameters (a_0, b_0, c_0, α, β, γ), local structure parameters (Average Bi−I bond length, $d_{av}^{\mathrm{Bi-I}}$, average non-adjacent I−Bi−I angle, Θ_{av}, average adjacent I−Bi−I angle, θ_{av}, and bismuth average effective coordination number, $\mathrm{ECN}^{\mathrm{Bi}}$), and the percent deviation between experimental and theoretical results, Δ.

	Exp.	DFT	Δ	DFT^{1A}	Δ	DFT^{1D}	Δ	DFT^{4A}	Δ	DFT^{4D}	Δ
a_0 (Å)	10.67	11.28	5.72	10.94	2.53	11.12	4.12	10.66	−0.09	10.86	1.78
b_0 (Å)	10.82	10.53	−2.68	10.71	−1.02	10.80	−0.18	10.68	−1.29	10.77	−0.46
c_0 (Å)	10.95	11.15	1.83	10.77	−1.64	10.57	−3.47	10.98	0.27	10.74	−1.92
α (°)	81.04	83.12	2.57	80.57	−0.58	81.05	0.01	81.17	0.16	81.76	0.89
β (°)	61.71	63.78	3.35	60.64	−1.73	60.37	−2.17	61.69	−0.03	61.47	−0.39
γ (°)	61.46	56.20	−8.56	60.88	−0.94	60.94	−0.85	61.80	0.55	61.84	0.62
$d_{av}^{\mathrm{Bi_1-I}}$ (Å)	3.08	3.10	0.65	3.10	0.65	3.11	0.97	3.10	0.65	3.11	0.97
$\Theta_{av}^{\mathrm{Bi_1}}$ (°)	180.00	177.20	−1.56	178.65	−0.75	178.64	−0.76	179.17	−0.46	177.94	−1.31
$\theta_{av}^{\mathrm{Bi_1}}$ (°)	90.00	89.99	−0.01	90.00	0.00	90.00	0.00	90.00	0.00	90.00	0.00
$\mathrm{ECN}^{\mathrm{Bi_1}}$	6.00	5.96	−0.67	5.97	0.50	5.98	−0.33	6.00	0.00	5.99	−0.17

Table S7: Experimental and theoretical values of lattice parameters (a_0, b_0, c_0, α, β, γ), local structure parameters (Average Bi−I bond length, $d_{av}^{\mathrm{Bi-I}}$, average non-adjacent I−Bi−I angle, Θ_{av}, average adjacent I−Bi−I angle, θ_{av}, and bismuth average effective coordination number, $\mathrm{ECN}^{\mathrm{Bi}}$), and the percent deviation between experimental and theoretical results, Δ.

	Exp.	DFT	Δ	DFT^{2A}	Δ	DFT^{2B}	Δ	DFT^{2E}	Δ	DFT^{4E}	Δ
a_0 (Å)	10.67	11.28	5.72	10.93	2.44	10.93	2.44	11.05	3.56	10.71	0.37
b_0 (Å)	10.82	10.53	−2.68	10.69	−1.20	10.72	−0.92	10.72	−0.92	10.74	−0.74
c_0 (Å)	10.95	11.15	1.83	10.77	−1.64	10.56	−3.56	10.67	−2.56	10.89	−0.55
α (°)	81.04	83.12	2.57	80.60	−0.54	80.49	−0.68	81.22	0.22	81.96	1.14
β (°)	61.71	63.78	3.35	60.59	−1.81	60.63	−1.75	60.27	−2.33	61.47	−0.39
γ (°)	61.46	56.20	−8.56	61.22	−0.39	61.04	−0.68	61.58	−0.19	62.18	1.17
$d_{av}^{\mathrm{Bi_1-I}}$ (Å)	3.08	3.10	0.65	3.10	0.65	3.10	0.65	3.11	0.97	3.11	0.97
$\Theta_{av}^{\mathrm{Bi_1}}$ (°)	180.00	177.20	−1.56	178.71	−0.72	178.69	−0.73	178.74	0.70	178.32	−0.93
$\theta_{av}^{\mathrm{Bi_1}}$ (°)	90.00	89.99	−0.01	90.00	0.00	90.00	0.00	90.00	0.00	90.00	0.00
$\mathrm{ECN}^{\mathrm{Bi_1}}$	6.00	5.96	−0.67	5.97	0.50	5.97	0.50	5.97	0.50	5.99	−0.17

Table S8: Lattice parameters ($a_0, b_0, c_0, \alpha, \beta,$ and γ for the crystal structure of 1, 2, and 3 perovskites. The error between theoretical (PBE plus vdW correction) and experimental values are given in %.

	Method	KD	SG	a_0 (Å)	b_0 (Å)	c_0 (Å)	α (°)	β (°)	γ (°)
	Exp.		$P\bar{1}$	8.83	10.70	11.79	114.45	99.70	100.09
	PBE	$1\times1\times1$	$P\bar{1}$	9.31	11.03	13.24	118.93	104.68	88.16
1	$\Delta E^{\mathrm{PBE}}_{\mathrm{KD=1}}$			5.44	3.08	12.30	3.91	4.99	−11.92
	PBE+D3	$1\times1\times1$	$P\bar{1}$	9.24	10.05	12.32	113.57	108.10	89.19
	$\Delta E^{\mathrm{PBE+D3}}_{\mathrm{KD=1}}$			4.64	−6.07	4.50	−0.77	8.43	−10.89
	PBE+D3	$2\times2\times2$	$P\bar{1}$	8.80	11.02	11.74	115.33	100.71	100.13
	$\Delta E^{\mathrm{PBE+D3}}_{\mathrm{KD=20}}$			−0.34	−0.09	−0.42	0.77	1.01	0.04
	Exp.		$Pna2_1$	23.55	10.43	21.92	90.0	90.0	90.0
	PBE	$1\times1\times1$	Pna21	23.93	11.21	22.42	90.0	90.0	90.0
2	$\Delta E^{\mathrm{PBE}}_{\mathrm{KD=1}}$			1.61	7.48	2.28	0.00	0.00	0.00
	PBE+D3	$1\times1\times1$	$Pna2_1$	23.32	10.34	21.86	90.0	90.0	90.0
	$\Delta E^{\mathrm{PBE+D3}}_{\mathrm{KD=1}}$			−0.98	−0.86	−0.27	0.00	0.00	0.00
	PBE+D3	$1\times2\times1$	$Pna2_1$	23.32	10.37	21.85	90.00	90.00	90.00
	$\Delta E^{\mathrm{PBE+D3}}_{\mathrm{KD=20}}$			−0.98	−0.58	−0.32	0.00	0.00	0.00
	Exp.		$P\bar{1}$	10.67	10.82	10.95	81.04	61.71	61.46
	PBE	$1\times1\times1$	$P\bar{1}$	11.22	10.46	11.30	80.92	63.44	63.03
3	$\Delta E^{\mathrm{PBE}}_{\mathrm{KD=1}}$			5.15	−3.33	3.19	−0.14	2.80	2.55
	PBE+D3	$1\times1\times1$	$P\bar{1}$	10.86	10.47	10.87	81.58	61.34	62.05
	$\Delta E^{\mathrm{PBE+D3}}_{\mathrm{KD=1}}$			1.78	−3.23	−0.73	0.66	−0.59	0.96
	PBE+D3	$2\times2\times2$	$P\bar{1}$	10.66	10.68	10.98	81.17	61.69	61.80
	$\Delta E^{\mathrm{PBE+D3}}_{\mathrm{KD=20}}$			−0.09	−1.29	0.27	0.16	−0.03	0.55

Table S9: Experimental and theoretical analysis: octahedra (Bi1/Bi2), average ($d_{av}^{\mathrm{Bi-I}}$) and standard deviation ($\sigma^{\mathrm{Bi-I}}$) of Bi−I bond length, average (Θ_{av}) and standard deviation (σ^{Θ}) of non-adjacent I−Bi−I angles, average (θ_{av}) and standard deviation (σ^{θ}) of adjacent I−Bi−I angles, octahedra volume (O_v), distortion index of bond length (DI), bond angle variance (BAV), and bismuth effective coordination number ($\mathrm{ECN^{Bi}}$).

	Method	KD ($\mathrm{Å}^{-1}$)	oct.	$d_{av}^{\mathrm{Bi-I}}$ (Å)	$\sigma^{\mathrm{Bi-I}}$ (Å)	Θ_{av} (°)	σ^{Θ} (°)	θ_{av} (°)	σ^{θ} (°)	O_v $\mathrm{Å}^3$	DI -	BAV ($^{\circ 2}$)	$\mathrm{ECN^{Bi}}$ NNN
1	Exp.		Bi1/Bi2	3.09	0.13	174.79	1.48	89.96	2.84	39.06	0.04	8.05	5.61
	PBE	$1\times1\times1$	Bi1/Bi2	3.15	0.20	175.19	2.02	90.05	4.88	41.07	0.04	23.80	5.36
	PBE+D3	$1\times1\times1$	Bi1/Bi2	3.14	0.22	174.37	2.65	90.00	7.09	40.11	0.05	50.20	5.28
	PBE+D3	$2\times2\times2$	Bi1/Bi2	3.11	0.11	174.83	1.95	89.97	3.04	40.02	0.03	9.23	5.74
2	Exp		Bi1	3.10	0.17	171.61	5.46	90.02	5.52	39.34	0.05	30.53	5.32
			Bi2	3.12	0.20	172.00	0.83	89.88	5.05	39.94	0.06	25.49	5.09
	PBE	$1\times1\times1$	Bi1	3.14	0.15	172.68	6.06	89.95	5.52	40.71	0.04	30.50	5.52
			Bi2	3.14	0.14	171.91	1.35	89.87	5.05	40.94	0.04	25.48	5.53
	PBE+D3	$1\times1\times1$	Bi1	3.12	0.16	170.63	3.99	90.08	5.94	40.01	0.04	35.33	5.44
			Bi2	3.13	0.16	172.37	0.66	89.89	4.82	40.49	0.04	23.25	5.41
	PBE+D3	$1\times2\times1$	Bi1	3.12	0.15	170.66	4.58	90.06	5.96	39.97	0.04	35.57	5.48
			Bi2	3.13	0.16	172.31	0.88	89.89	4.76	40.47	0.04	22.68	5.40
3	Exp.		Bi1	3.08	0.01	180.00	0.00	90.00	1.91	38.94	0.00	3.65	6.00
	PBE	$1\times1\times1$	Bi1	3.15	0.02	179.22	0.74	90.00	1.87	41.44	0.01	3.49	5.99
	PBE+D3	$1\times1\times1$	Bi1	3.12	0.01	179.30	0.06	90.00	1.65	40.58	0.00	2.72	5.99
	PBE+D3	$2\times2\times2$	Bi1	3.10	0.02	179.17	0.40	90.00	2.18	39.69	0.00	4.77	5.99

2.2 Total and Local Density of States

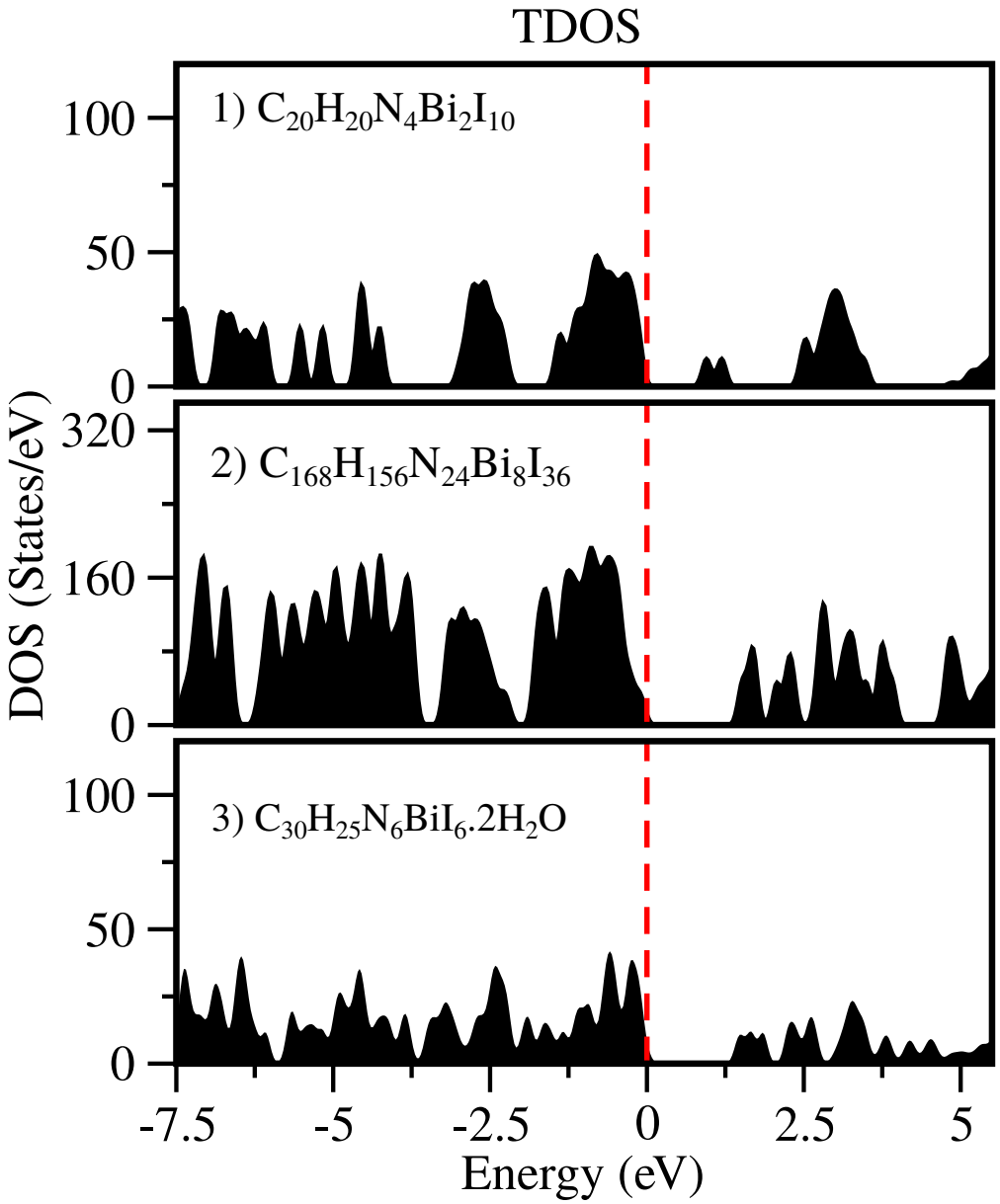

Figure S21: Total density of states (TDOS) for PBE+D3 optimized 1, 2, and 3 hybrid-perovskites. The fundamental band gap obtained in this calculations are (i) **1** $= 0.9802\,\mathrm{eV}$ (ii) **2** $= 1.5300\,\mathrm{eV}$**, and** (iii) **3** $= 1.406\,\mathrm{eV}$**.**

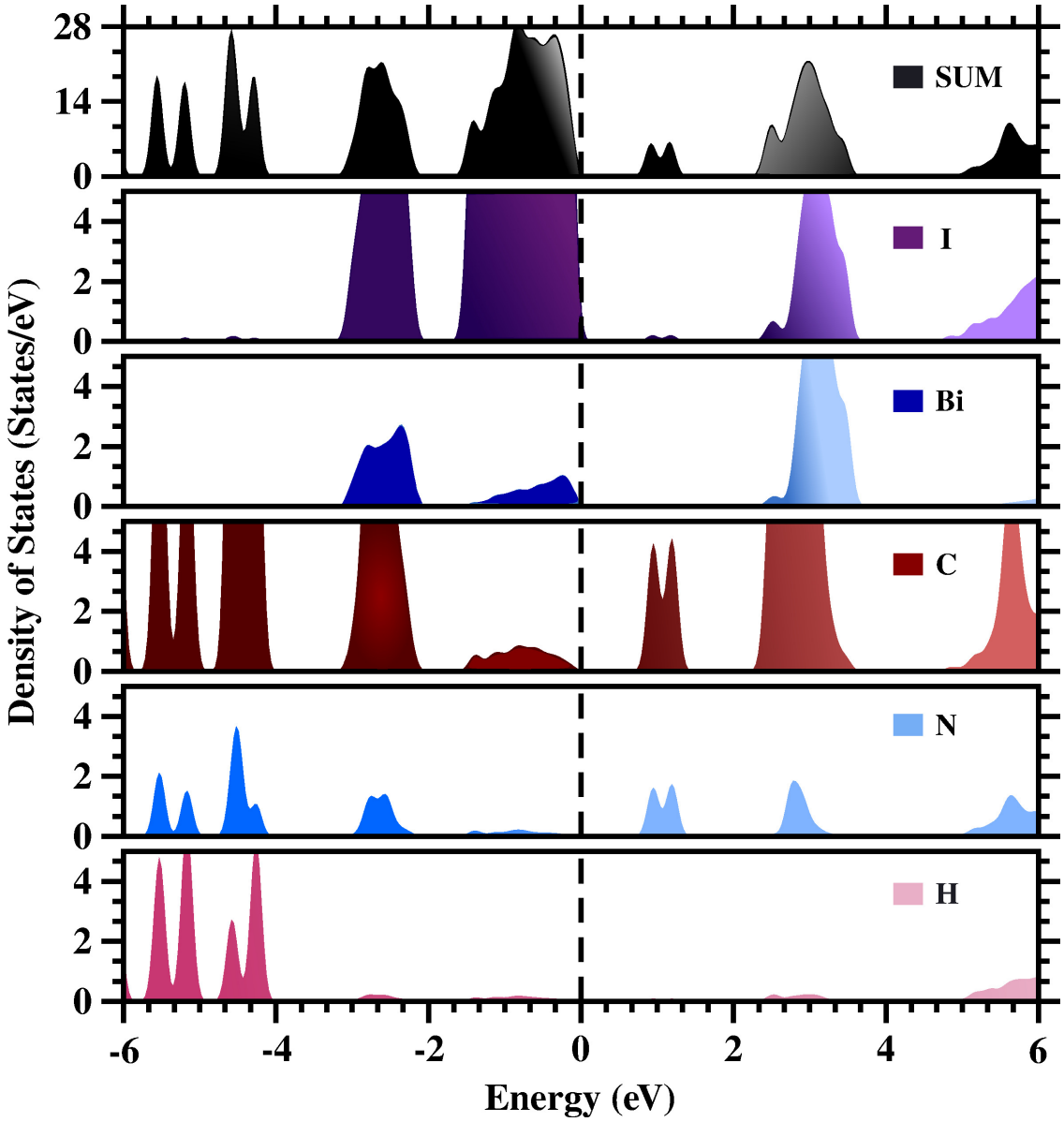

Figure S22: Perovskite 1: ($C_{20}H_{20}N_4Bi_2I_{10}$) Density of states obatined with PBE+D3. Fundamental band gap is $0.9802\,\mathrm{eV}$.

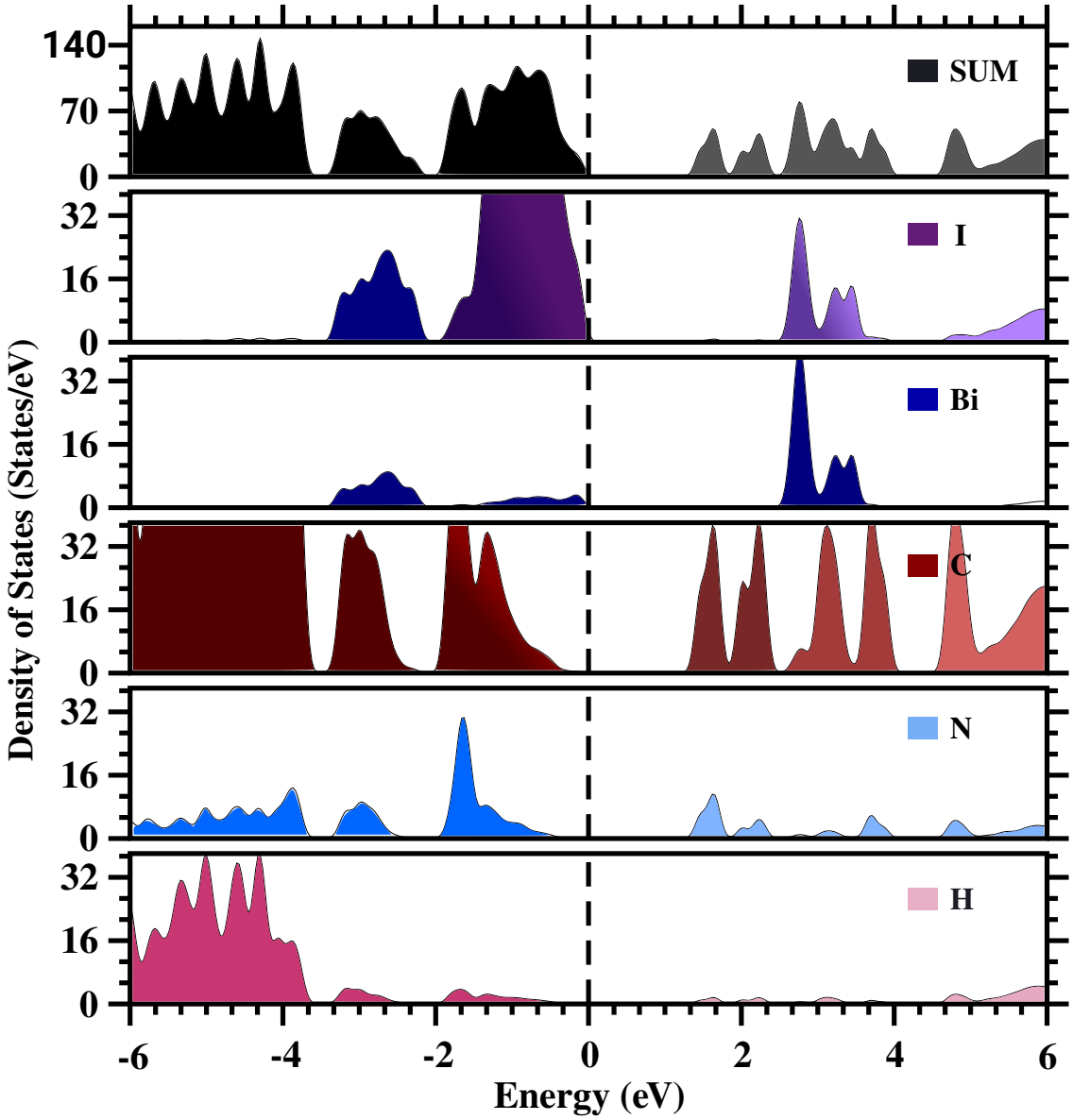

Figure S23: Density of states obtained with PBE+D3 for Perovskite 2. The fundamental band gap is 1.5300 eV**.**

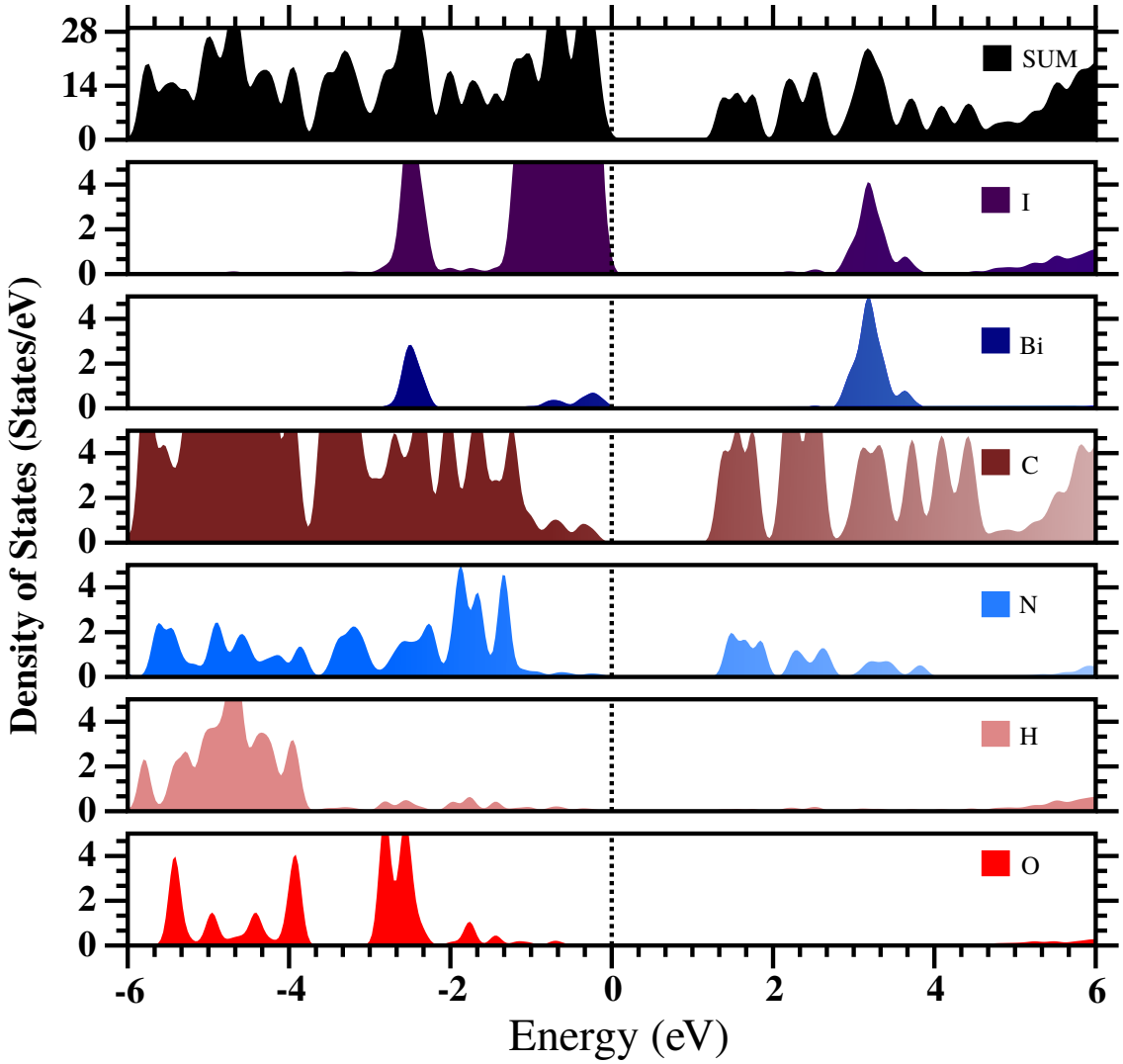

Figure S24: Density of states obtained with PBE+D3 for perovskite 3. The fundamental band gap is 1.406 eV.

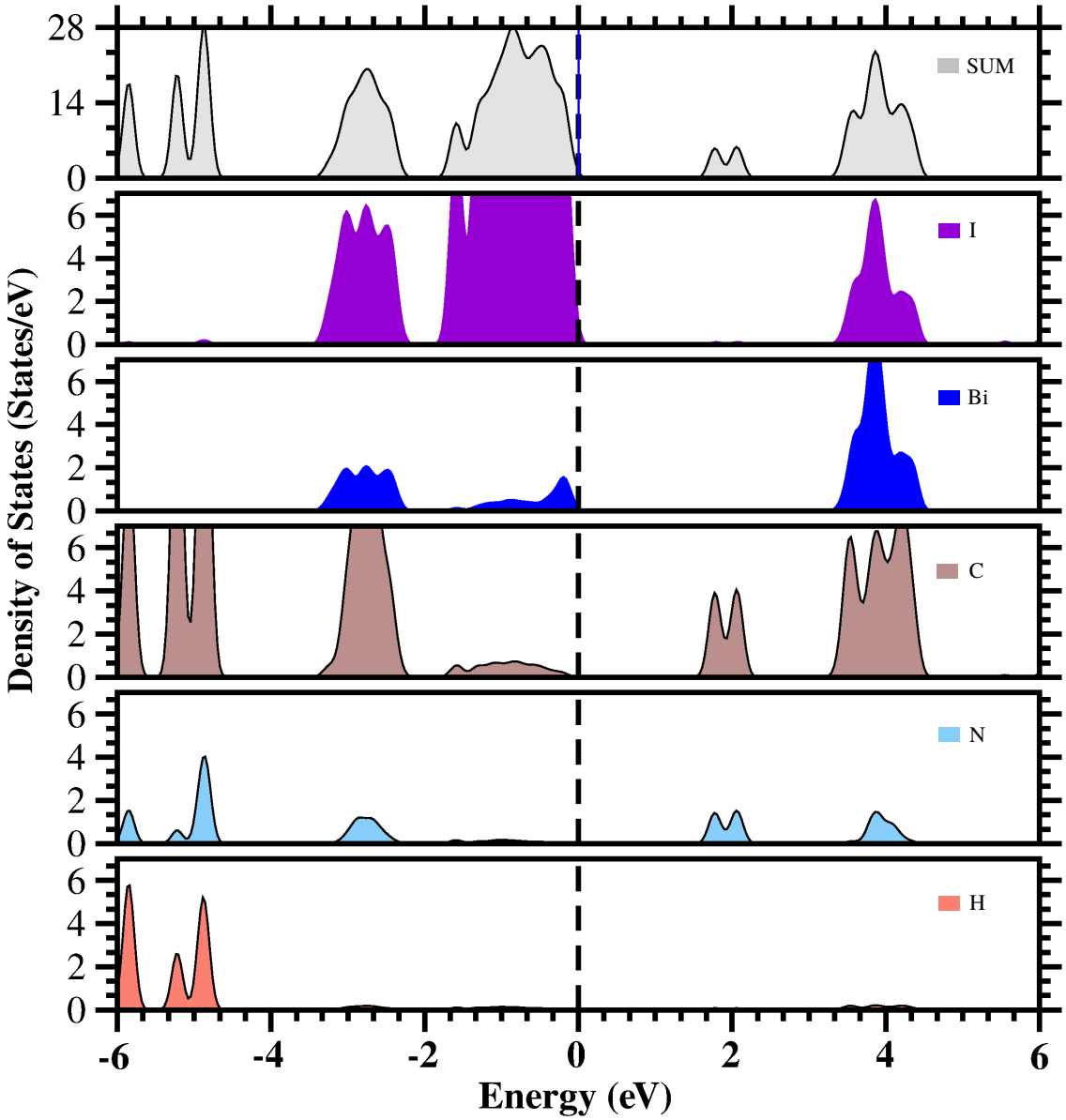

Figure S25: Density of states obtained with HSE06 for perovskite 1. The fundamental band gap is of 1.8004 eV

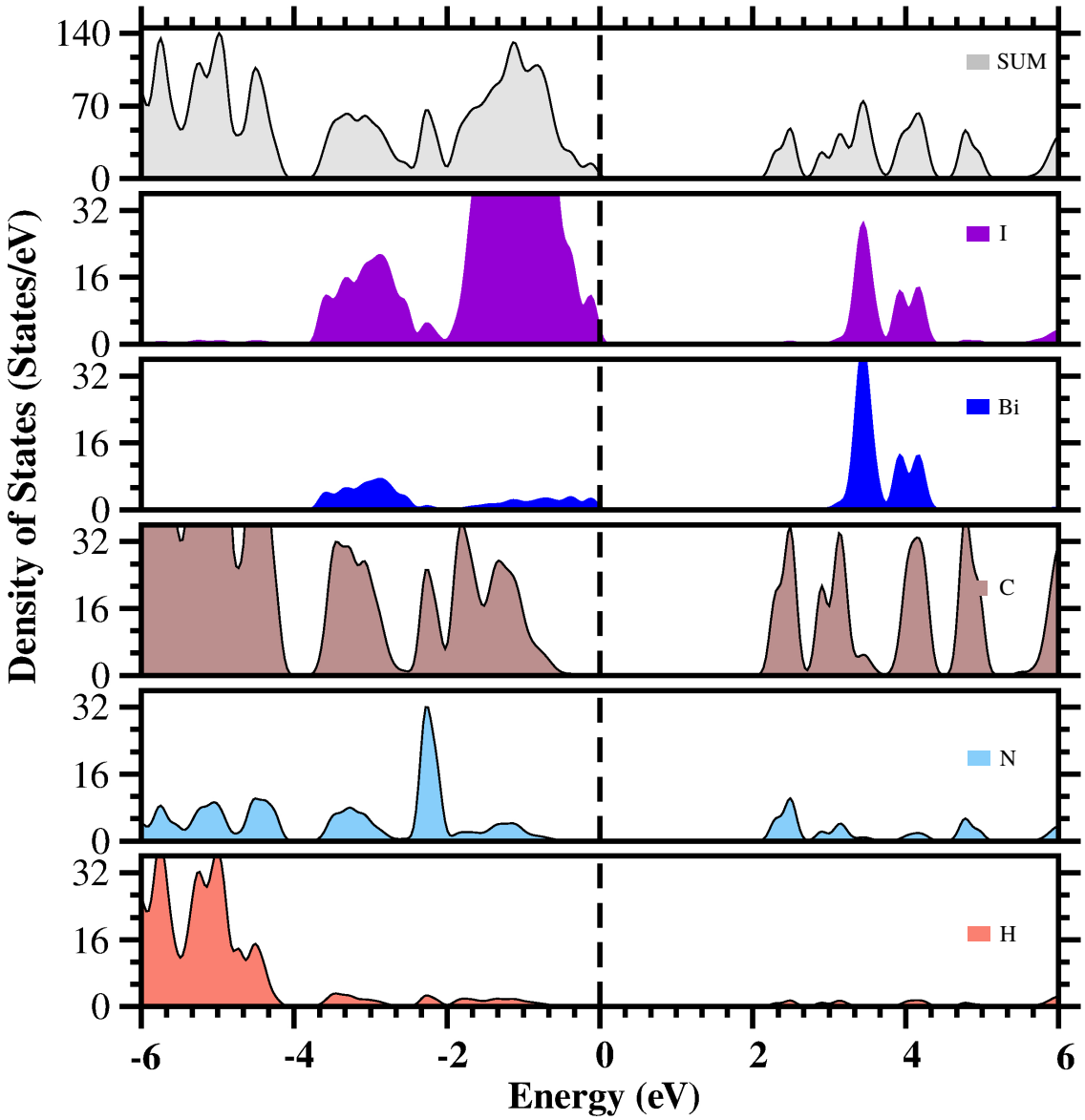

Figure S26: Density of states obtained with HSE06 for perovskite 2. The fundamental band gap is of 2.3525 eV

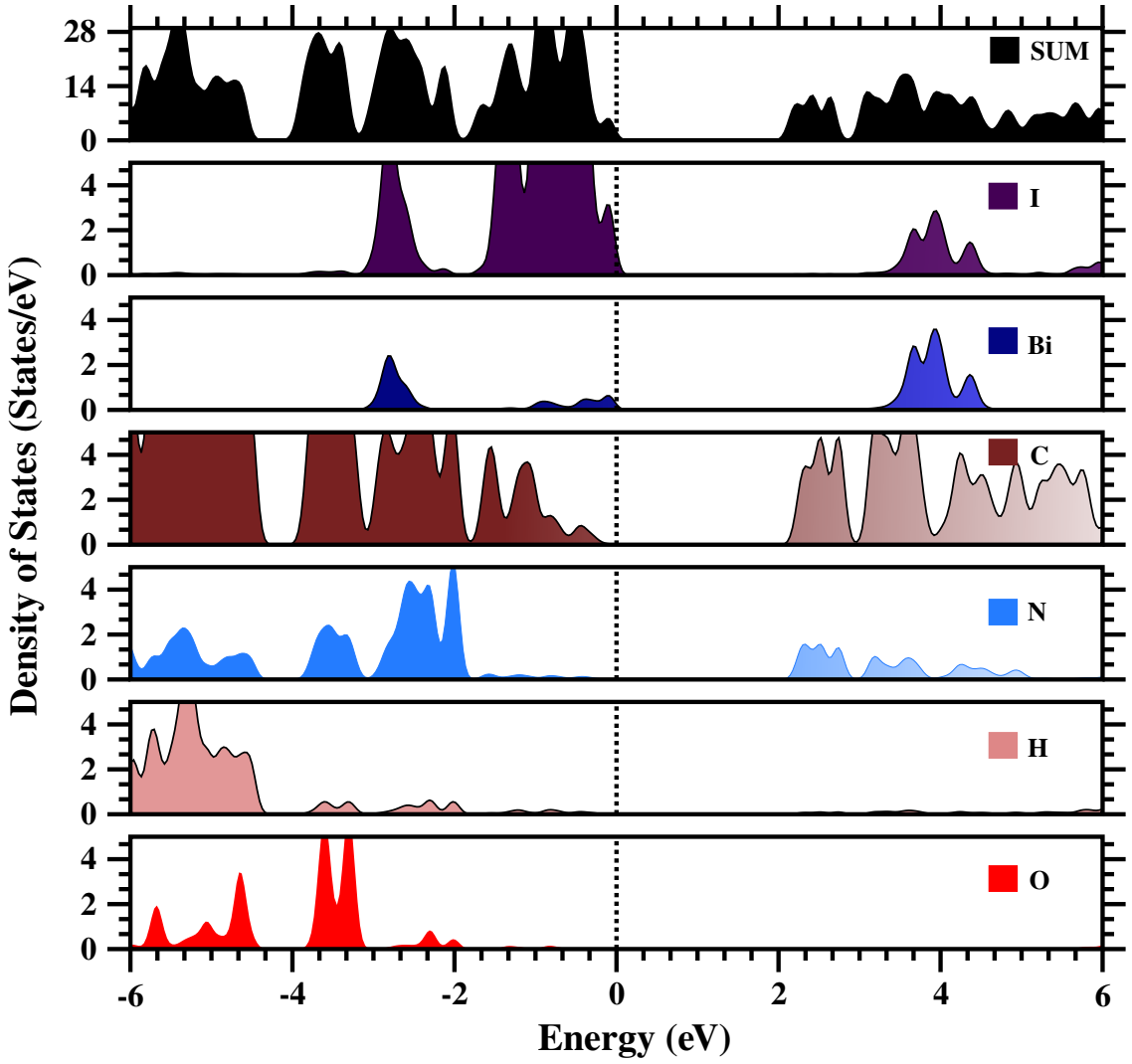

Figure S27: Density of states obtained with HSE06 for perovskite 3. The band gap is 2.24 eV

2.3 Band Structures

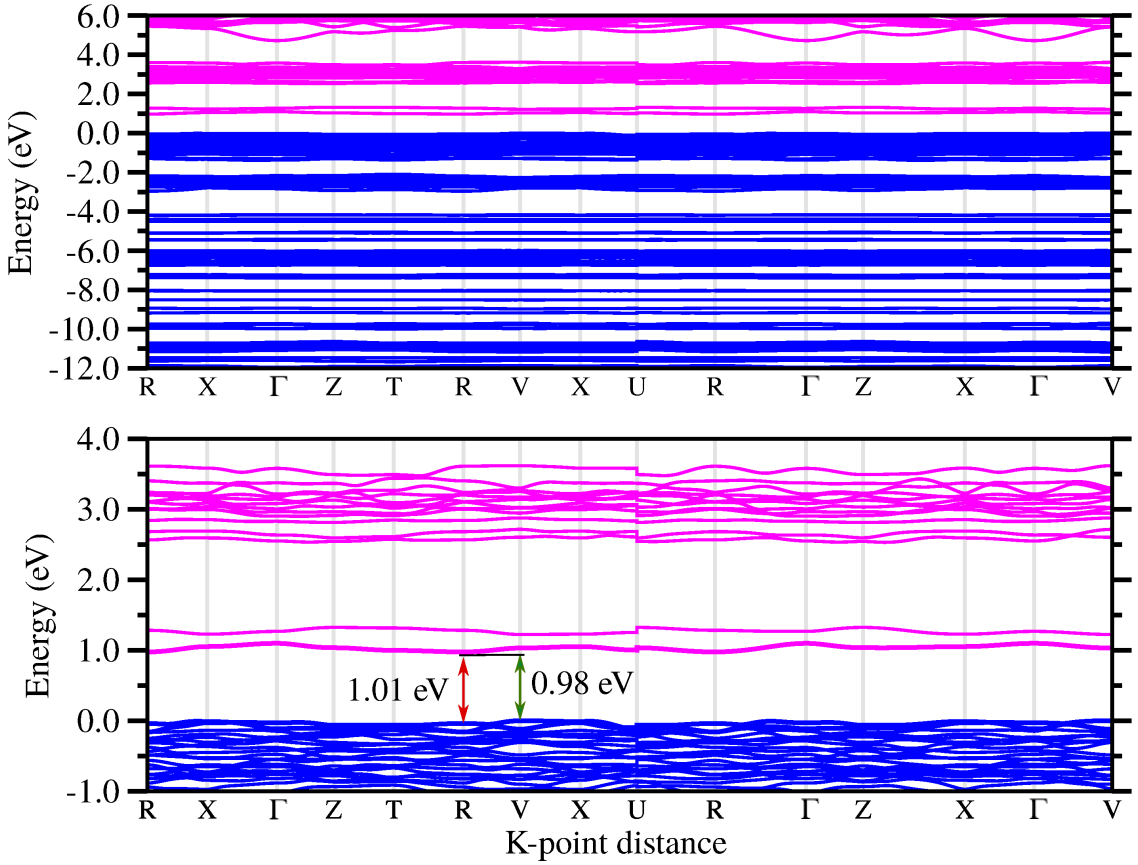

Figure S28: Band structure of perovskite 1 obtained with PBE+D3. The indirect fundamental band gap is $0.9756\,\mathrm{eV}$ **with the top of valence band at V point and the bottom of conduction band at R point. The direct fundamental band gap is** $1.0143\,\mathrm{eV}$ **and occurs at R point.**

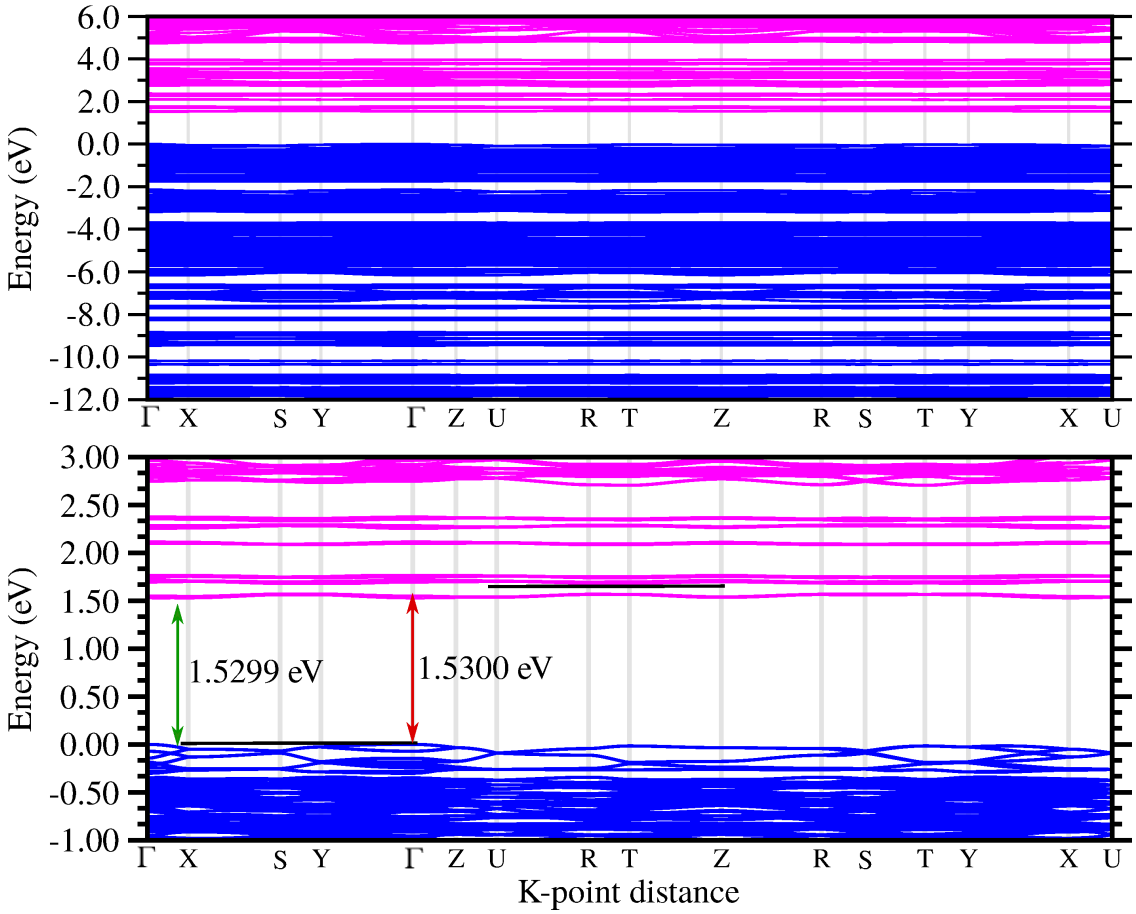

Figure S29: Band structure of perovskite 2 obtained with PBE+D3. The indirect fundamental band gap is of $1.53\,\mathrm{eV}$ with the top of valence band at Γ point and the bottom of conduction band in three degenerated points located between the path of Γ and X. The fundamental direct band gap is $1.53\,\mathrm{eV}$ and occurs at Γ point.

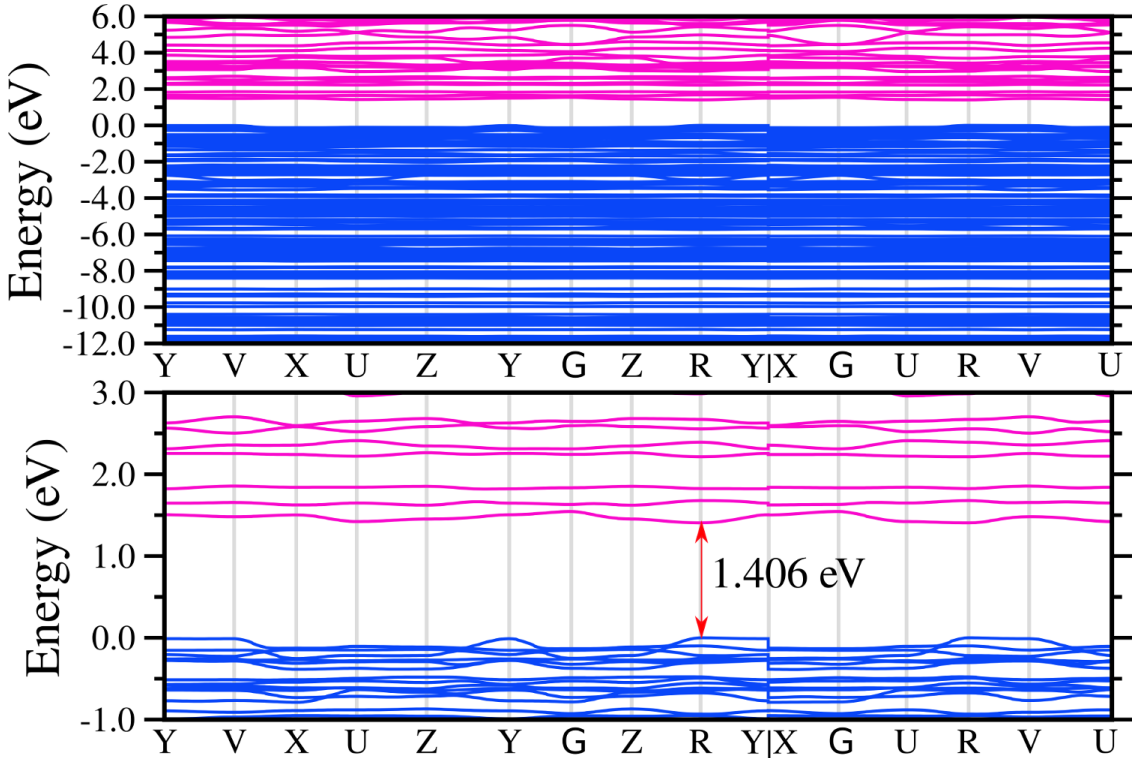

Figure S30: Band structure of perovskite 3 obtained with PBE+D3. Direct fundamental band gap of 1.406 eV **at R point.**

References

(S1) Chen, W.-J.; Chu, K.-B.; Song, J.-L. Low-dimensional bismuth(III) Iodide Hybrid Material with High Activity for the Fast Removal of Rhodamine B. *Acta Crystallogr., Sect. C: Cryst. Struct. Commun.* **2018**, *74*, 1744–1749.

(S2) Da Silva, J. L. F. Effective Coordination Concept Applied for Phase Change $(GeTe)_m(Sb_2Te_3)_n$ Compounds. *J. Appl. Phys.* **2011**, *109*, 023502.

(S3) Robinson, K.; Gibbs, G. V.; Ribbe, P. H. Quadratic Elongation: A Quantitative Measure of Distortion in Coordination Polyhedra. *Science* **1971**, *172*, 567–570.

(S4) Baur, W. H. The Geometry of Polyhedral Distortions. Predictive Relationships for the Phosphate Group. *Acta Crystallogr., Sect. B: Struct. Sci.* **1974**, *30*, 1195–1215.